ACS EARTH AND SPACE CHEMISTRY

http://pubs.acs.org/journal/aesccq Article

# Nanoscale Infrared Characterization of Dark Clasts and Fine-Grained Rims in CM2 Chondrites: Aguas Zarcas and Jbilet Winselwan

Mehmet Yesiltas,* Timothy D. Glotch, and Melike Kaya

Cite This: *ACS Earth Space Chem.* 2021, 5, 3281−3296 Read Online



**ABSTRACT:** Carbonaceous chondrites are among the most primitive meteorites that escaped extreme temperatures and melting in their parent bodies and, as such, offer valuable records of the parent body origins, formation, and evolution. The presence of organic molecules and carbonaceous phases make CM chondrites invaluable as they may have contributed prebiotic material to early Earth. Fine-grained rims (FGRs) and organic-rich dark clasts are particularly interesting features, the origin, formation, and evolution of which are not fully understood. In this study, we aimed to characterize several FGRs and dark clasts in two CM2 chondrites, Aguas Zarcas and Jbilet Winselwan, using backscattered electron images, confocal micro-Raman spectroscopy, and nanoscale near-field infrared imaging and spectroscopy. The nano-FTIR spectra show that the dark clasts and FGRs are chemically heterogeneous at a submicron scale and those of Aguas Zarcas are composed of organics (such as aliphatics, aromatics, and carbonyls) as well as alteration phases (such as phyllosilicates, carbonates, and sulfates). The FGRs are compositionally almost identical and exhibit heterogeneous alteration as well as a lack of fragmentation. The thicknesses of FGRs positively correlate with the enclosed chondrule diameter regardless of the chondrule type. The samples appeared to have experienced minimal brecciation after the chondrules were surrounded by the FGRs. These observations suggest nebular origin for the FGRs. The presence of organics embedded within these FGRs may further indicate that they may have formed in the solar nebula as well. In comparison, Jbilet Winselwan contains relatively less organics and exhibits more thermally metamorphosed mineralogy and matrix textures. These features could be the result of short-duration heating, such as impact heating, which also likely caused shock and dehydration/decomposition of the hydrated phases.

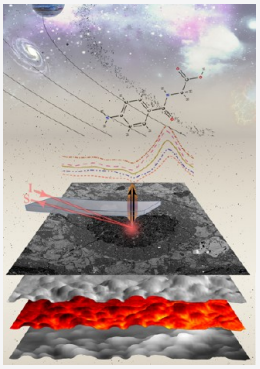

**KEYWORDS:** *carbonaceous chondrites, fine-grained rims, dark clasts, organic matter, nanoscale, infrared, spectroscopy*



## ■ INTRODUCTION

Carbonaceous chondrites are some of the most primitive meteorites that escaped extreme temperatures and melting in their parent bodies. The Mighei-type carbonaceous chondrites (CM chondrites) are especially interesting samples because they preserve records of their origin, formation, and evolution. Some of their constituents include primary coarse-grained and high-temperature phases, such as chondrules, Fe−Ni opaque phases, and anhydrous silicates. CM chondrites also contain secondary phases, such as phyllosilicates, oxides, and sulfates,[1,2] that formed as a result of diverse aqueous alteration processes that took place in the parent body. The presence of organic molecules and carbonaceous phases in CM chondrites make them particularly invaluable for research as they may have contributed prebiotic material to early Earth. Therefore, many studies have focused on the petrology, composition, and spectroscopic characteristics of CM chondrites and provide important insights into pre- and postaccretionary processes and their resulting effects on chemical composition (e.g., refs 3−20).

Other significant features of CM chondrites are their fine-grained rims (FGRs) and organic-rich dark clasts. FGRs have been the subject of much research (e.g., refs 1, 5, 17, 21−31) and mostly occur around chondrules (usually enclosing the entire chondrule), calcium−aluminum-rich inclusions, and minerals.[5,25,26,28,32] Although some differences exist, the FGRs and the matrices in CM chondrites are compositionally similar, including low-temperature phyllosilicates and organic materials.[31] Indeed, in some cases, FGRs and matrices are mineralogically indistinguishable.[1,29] On the contrary, their grain size, porosity, presolar grain abundance, and texture can vary.[5,30]

On the basis of these petrological, compositional, and textural differences and similarities, several scenarios have been proposed for the origin of FGRs. The "solar nebula" and "parent body" origin models are the two main possibilities. In the solar nebular model, FGRs form *via* the accretion of dust onto the surfaces of chondrules.[5,21,26,30,32−42] In the parent body model, FGRs are formed *via* processes such as alteration, metamorphism, compaction, gardening, etc.[24,38,43−46] An alternative

**Special Issue:** Chemical Complexity in Planetary Systems

**Received:** August 15, 2021
**Revised:** November 5, 2021
**Accepted:** November 8, 2021
**Published:** November 16, 2021

possibility is formation *via* the accretion of the dust onto the chondrules in the solar nebula and aqueous alteration in the CM chondrite parent body.[1,25,38,44,47] As such, the origin of FGRs remains controversial and is a matter of considerable ongoing debate.

Dark clasts are present in many different types of meteorites including chondrites and achondrites.[48−54] Dark clasts are usually carbon- and organic-rich and are often foreign to the host meteorite (i.e., xenolithic clasts in ordinary chondrites[51,52,54] and howardites.[49,53] On the contrary, the organic matter in CM chondrites is usually present in their matrices and that the dark clasts in CM chondrites may host more carbon, thus organic matter, compared to the matrix.

CM chondrites are the most abundant carbonaceous chondrites and are mostly aqueously altered to different degrees. They are rich in water and contain abundant secondary minerals formed through the alteration of anhydrous precursor phases in the parent body. Thus, many insights into parent body aqueous alteration processes, as well as the characteristics of alteration products, have been obtained through the petrologic and spectroscopic study of CM chondrites (e.g., refs 12, 13, and 44 Most CM chondrites are classified as petrologic type 2 (CM2), indicating that their matrices are fully hydrated[55] and the primary anhydrous mineralogy is only partially hydrated.[56] It is believed that accreted extraterrestrial ices melted on the parent body and mediated complex aqueous alteration on the CM chondrite parent bodies (e.g., ref 56). The oxygen isotopic composition of water released from phyllosilicates[57] and the clumped-isotope thermometry of carbonates in the CM chondrites[58,59] suggest that the aqueous alteration on the CM parent body occurred at temperatures <100 °C and lasted about 10 Ma (based on carbonate Mn−Cr ages).[60−62] On the contrary, some CM chondrites exhibit evidence of thermal heating after having undergone aqueous alteration.[63−65] In fact, the produced heating for some CM chondrites was sufficiently high to dehydrate and recrystallize the alteration products previously formed through the aqueous alteration processes.[14,66,67] In addition, this heating also caused carbonaceous matter to become graphitic through graphitization and carbonization reactions.[68]

Aguas Zarcas is a relatively new carbonaceous chondrite that fell in Costa Rica in 2019.[69] This meteorite is a brecciated and highly aqueously altered CM2 chondrite comprising several distinct lithologies. It consists predominantly of phyllosilicates and is rich in water and organics;[70,71] at least five different lithologies were recently identified by Kerraouch et al.[71] including chondrule-poor, chondrule-rich, metal-rich, and CI-like lithologies. The metal-rich lithology is dominated by metals, sulfides, olivine, pyroxene, and carbonate.[71] A significantly high abundance of carbonates (>50 vol %) is found in some Ca, Al-rich inclusions (CAIs) of Aguas Zarcas.[72]

Jbilet Winselwan was found in the Western Sahara in 2013 and is also a brecciated CM2 chondrite. However, unlike Aguas Zarcas, Jbilet Winselwan exhibits evidence of aqueous alteration followed by significant impact-heating,[65,73−75] evident from the presence of dehydrated phyllosilicates, recrystallized olivine, and melted Fe-sulfide.[65] Furthermore, the presence of a "spongy" matrix texture, melted troilite, and partially evaporated sulfur in some of the lithologies of Jbilet Winselwan suggests that this CM2 chondrite experienced flash heating at some point in the parent body.[65] On thte basis of the X-ray diffraction (XRD) patterns of heated carbonaceous chondrites and the heating stage (I−IV) scheme of Nakamura et al.,[76] Jbilet Winselwan was classified as a stage-II chondrite, suggesting a heating temperature range of 250−500 °C.[76] The findings of King et al.,[74] which show the sharp XRD peaks of olivine typical of unheated CM chondrites, also suggest heating temperatures of <500 °C.

The unique textures, mineralogies, and compositional heterogeneities of Aguas Zarcas and Jbilet Winselwan make them valuable candidates for investigating the molecular functional groups within materials that originate from the solar nebula and/or parent asteroids. This includes the FGRs and dark clasts that are characteristic of CM chondrites. Their characterization is, thus, important for understanding the chemistry and accretionary history of carbonaceous chondritic materials in the early solar system. The thickness of FGRs is typically in the order of 100 $\mu$m, which is thick enough to enable characterization using a variety of bulk analytical techniques; however, these rims are not always homogeneous. Indeed, the FGRs in CM2 chondrites are compositionally extremely heterogeneous.[21] This is partly due to the fact that they display features of both the accretion of well-mixed dust grains (<1 $\mu$m) and subsequent aqueous alteration.[25] Furthermore, the extremely small grain size of FGRs (<1 $\mu$m) makes their characterization difficult and challenging.[23,25] The majority of water in CM chondrites is present within phyllosilicates, which are typically 10−100 nm in size within FGRs.[26] Evidently, analytical techniques with nanoscale spatial resolution are required to characterize FGRs and dark phases in carbonaceous chondrites, such as Aguas Zarcas and Jbilet Winselwan. In addition, the mechanism, timing, and duration of the metamorphic events that produced the heated CM chondrites remain poorly constrained.

In this study, we aimed to investigate and characterize several FGRs and dark phases in pristine samples of Aguas Zarcas and Jbilet Winselwan using nanoscale Fourier-transform infrared (nano-FTIR) spectroscopy, which complements studies of other rimmed chondrules and dark clasts identified elsewhere.

## ■ EXPERIMENTAL SECTION

**Samples.** Many pieces of Aguas Zarcas were recovered within a week of the fall. Some of the samples were quickly recovered such that they avoided rainfall in the fall location. As terrestrial water contamination would be a serious problem for our investigation, a prerain Aguas Zarcas specimen was acquired from a private collection, as was our Jbilet Winselwan sample. A chip of each meteorite was broken off from the interior of the larger (∼3 gr) specimens and prepared as a polished thick section. In our scanning electron microscopy (SEM) investigations, we did not observe grain corrosion or rust, which suggests minimal terrestrial weathering of the samples.

**Electron Microscopy.** We used a Zeiss LS-10 EVO SEM coupled with a backscattered electron (BSE) detector to acquire the compositional data as well as BSE images of the samples. Individual BSE images of samples were collected at an accelerating voltage of 20 kV with a beam current of 20 nA and a working distance of 10 mm at small (∼80−100× ) magnification. Such images were then merged to create the large size mosaic BSE images of the two meteorites. Utilizing energy dispersive spectroscopy (EDS), we also collected elemental spectra of several rims and the matrix.

**Nano-FTIR Spectroscopy.** Nano-FTIR spectroscopy is based on scattering-type scanning near-field optical microscopy (s-SNOM).[77] A conductive metal-coated atomic force microscope (AFM) tip, which is illuminated by broadband infrared radiation, probes and measures the molecular vibrations within


https://doi.org/10.1021/acsearthspacechem.1c00290
ACS Earth Space Chem. 2021, 5, 3281−3296

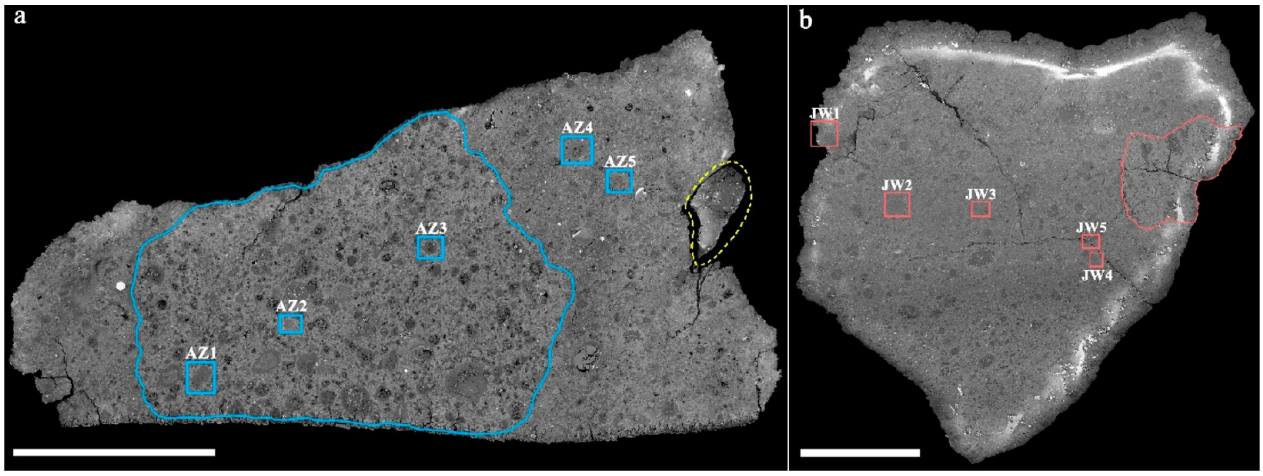


**Figure 1.** BSE images of the studied CM2 chondrites, (a) Aguas Zarcas and (b) Jbilet Winselwan. White scale bars are ∼0.5 cm long. Rectangles denote the regions studied *via* nano-FTIR spectroscopy. Blue and light-red lines outline the different lithologies observed in the samples. The yellow dashed line in (a) shows the only metal-rich lithology we observed in Aguas Zarcas.

the measurement area with its apex. Thus, the spatial resolution of the measurements is generally equal to the radius of curvature of the probing tip.

In this work, we used a commercial s-SNOM nano-FTIR spectroscopy system (neaspec GmbH) equipped with multiple mid-infrared broadband lasers to acquire nano-FTIR spectra of the samples. The spectra were collected from the selected points within the 1600−650 $cm^{-1}$ spectral range with a ∼20 nm spatial resolution and a 12 $cm^{-1}$ spectral resolution. For each spectrum, 30 spectra (each with 10 ms integration time) were accumulated and coadded. AFM scans were collected using a commercial (neaspec GmbH) metalized (Pt-coated) cantilever tip with a resonance frequency of 250−270 kHz, which was used to map the surface topography. Each spectrum was automatically calibrated at the end of spectrum collection with a reference spectrum obtained on a silicon wafer prior to the sample measurement.

The nano-FTIR spectroscopy system measures amplitude (reflectance) and phase (absorbance) spectra simultaneously. The latter is used here as the infrared absorbance of the studied samples. During each spectral measurement, the AFM tip scans the surface and creates multiple images, each representing a different property of the surface. Mechanical amplitude and optical amplitude images are among the most commonly used among scientists and the most meaningful images for interpretation.[54,78−80] These amplitude images represent topography (i.e., the height of the AFM tip relative to the sample surface) and reflectivity (i.e., broadband reflectivity integrated across the full wavelength range), respectively. In some cases, the studied region is better visualized/characterized when the two amplitude images are overlaid onto each other. This also helps associate the spatial/petrographic context with the reflectivity of the considered region.

**Confocal Micro-Raman Spectroscopy.** Raman spectroscopic measurements were conducted using a commercial confocal Raman microspectroscopy system (WiTec alpha300R) equipped with a 600 g/mm grating, 532 nm Nd:YAG laser, and a 50× objective (NA = 0.8). We calibrated the spectrograph using a silicon wafer substrate prior to measurements. Individual Raman spectra of predetermined spots were acquired with a 1 s integration time for 60 accumulations within 800−2000 $cm^{-1}$. Throughout the data acquisition, the power density of the circular ∼0.8 $\mu$m diameter laser beam was ∼0.2−0.5 mW/$\mu m^2$ on the sample surface. Upon data collection, we reduced the collected spectra using the commercial ProjectPLUSv4 (WiTec GmbH) software package. We first removed artificial fluorescence background from the spectra by subtracting a polynomial with a shape size of 200 and a noise factor of 2. To derive Raman spectral parameters of the first order carbon bands, we fitted the background-removed spectra with a pair of Lorentzian functions (e.g., refs 53, 54, 81, and 82).

## ■ RESULTS AND DISCUSSION

Although several regions of interest were identified, we limited our investigation to the five regions in each meteorite indicated by rectangular boxes in Figure 1. In the case of the Aguas Zarcas sample, a distinct lithology (relatively dark in color, indicated by a blue line in Figure 1a) was observed to be embedded in another lithology that appeared brighter in the BSE image. This darker lithology is relatively rich in chondrules. In comparison, the brighter lithology contains mineral fragments and a smaller number of chondrules. The entire Aguas Zarcas section appears to be metal-poor except for a very small (0.2 cm) piece that can be seen to be completely separated from the main section (on the far right in Figure 1a).

The Jbilet Winselwan sample also lacks metals. The BSE image in Figure 1b shows a distinct lithology (enclosed by a light-red line) with a "spongy" matrix texture. This indicates a short duration of significant heating (such as flash heating).[65] The FGRs within this "spongy" lithology are less abundant and less distinct compared to those within the main lithology. We note that the polished sections were imaged by SEM without a conductive coating, which would otherwise have prevented subsequent nano-FTIR spectroscopic measurements. The lack of conductive coating resulted in the accumulation of charges around the Jbilet Winselwan sample, which was seen as artificial bright white bands—these bands do not indicate metal.

In Figure 2, we show some of the FGRs and dark clasts identified in our sections of Aguas Zarcas and Jbilet Winselwan. Most FGRs completely enclose chondrules, although few incomplete rims are also present. Those regions labeled as AZ1−AZ5 and JW1−JW5 are selected for nano-FTIR investigation in this study.


https://doi.org/10.1021/acsearthspacechem.1c00290
ACS Earth Space Chem. 2021, 5, 3281−3296

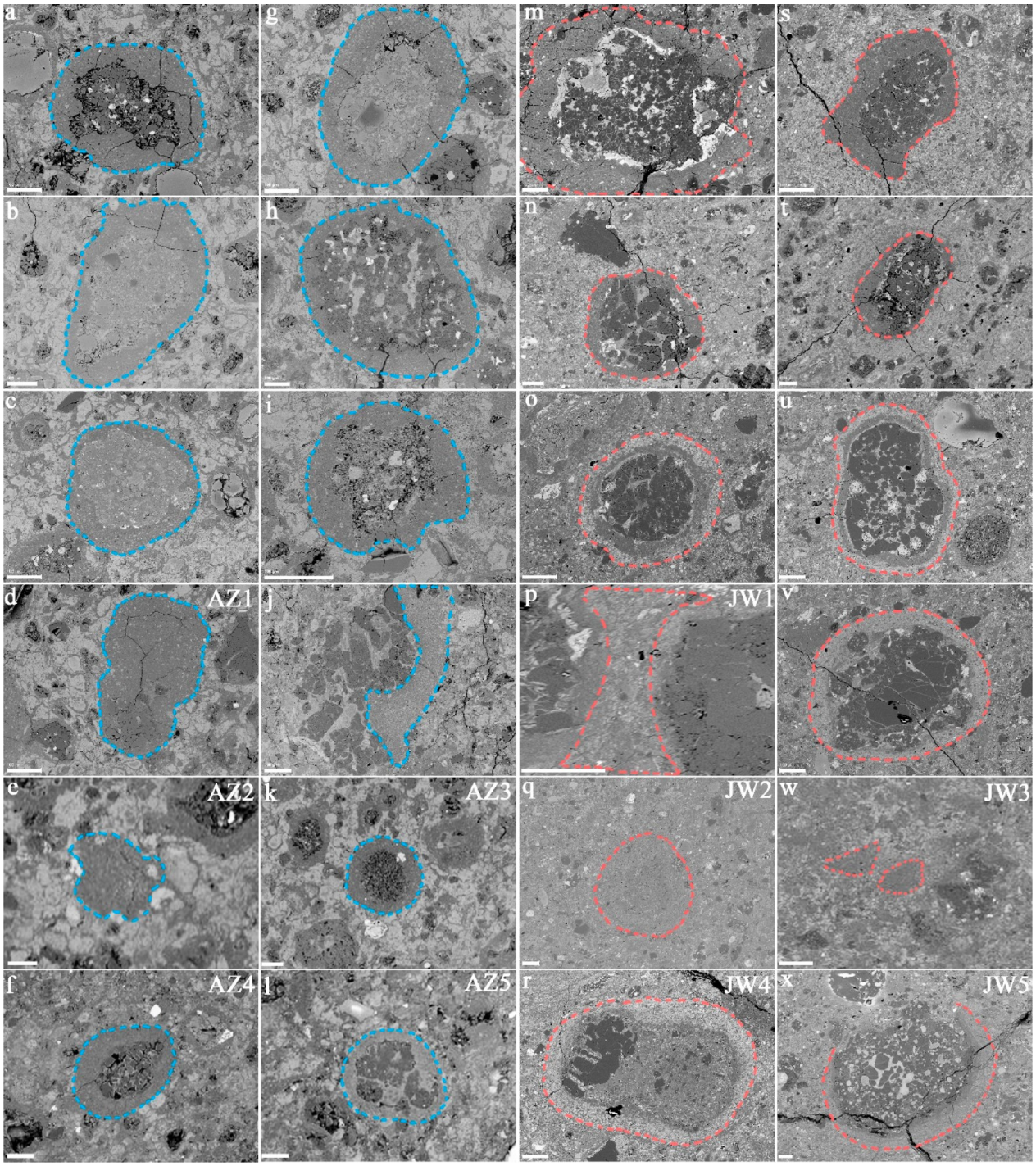


**Figure 2.** BSE images of various dark phases and FGRs in Aguas Zarcas (left panel, a–l) and Jbilet Winselwan (right panel, m–x). The dashed lines outline the observed dark phases, and FGRs that enclose different types of chondrules in both CM2 chondrites. The regions studied *via* nano-FTIR are labeled as AZ1–AZ5 and JW1–JW5, respectively.

**Nano-FTIR Spectral Results for Aguas Zarcas.** Region-AZ1 (Figure 2d) contains a dark clast set within a brighter matrix material (Figure 3a,b). The bright and dark regions in the AFM optical amplitude image (Figure 3c) indicate the presence of chemically different materials. A total of 16 nano-FTIR spectra were collected from the central part of the dark phase. The averaged spectrum exhibits bands at 1615, 1515, 1440, 1350, 1175, and 1045 $cm^{-1}$ due to the presence of organic and inorganic components (Figure 3f). The bands at 1615 and 1515 $cm^{-1}$ are due to C═C vibrational modes in aromatic hydrocarbons.[81,83,84] The peak at 1440 $cm^{-1}$ is attributed to $CO_3^{2-}$ ions within carbonates.[84−86] The peak at 1350 $cm^{-1}$ is due to C—H vibrational modes in aliphatic hydrocarbons. The averaged spectrum also shows inorganic peaks, such as a weak shoulder peak at 1175 $cm^{-1}$, which is possibly due to $SO_4^{2-}$ vibrational modes in sulfates[81,84,87] and a more intense and broader peak at 1045 $cm^{-1}$ due to Si—O vibrational modes in silicates.[87] The individual nano-FTIR curves shown in Figure 3g show some spectral variation. For instance, a small feature at 1560 $cm^{-1}$ (possibly due to C═C vibrational modes in


https://doi.org/10.1021/acsearthspacechem.1c00290
ACS Earth Space Chem. 2021, 5, 3281−3296

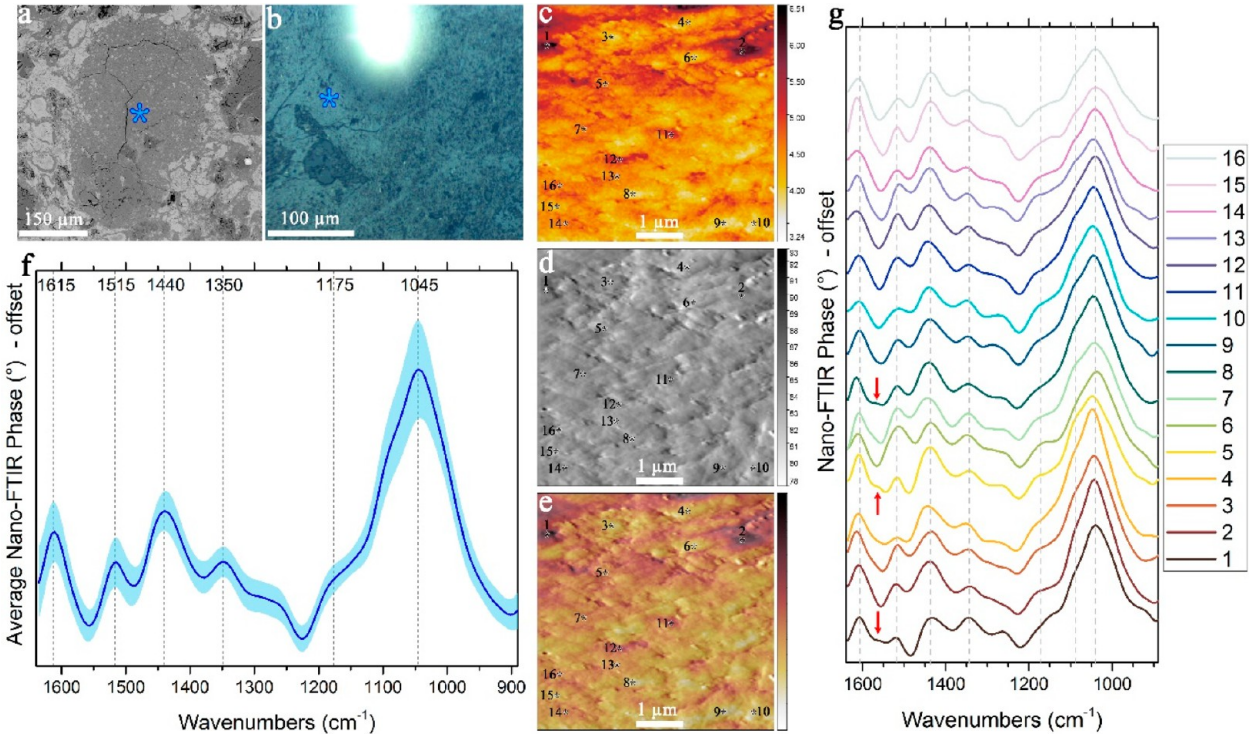


**Figure 3.** (a) BSE and (b) white-light images of Region-AZ1. Blue stars denote the studied location. AFM (c) optical, (d) mechanical, (e) amplitude, and overlaid images indicate the spots where nano-FTIR spectra were collected. (f) Average and (g) individual nano-FTIR spectra show positions of bands attributed to organics and minerals. The light-blue area in (f) is the standard deviation of the collected spectra.

aromatics) is present in spectra #1, #5, and #8 (red arrows) but is absent in the others. Similarly, the sulfate peak at 1175 $cm^{-1}$ is weak in some spectra but strong in others, indicating varying sulfate abundance even within a small area. The 1515 $cm^{-1}$ peak due to aromatic hydrocarbons also varies from point to point, being weakest in spectrum #4 and strongest in spectrum #6 (Figure 3g).

Figure 4 shows our results for another dark phase (Region-AZ2, Figure 2e) present in Aguas Zarcas. For this region, both the dark phase (blue/green star) and the nearby brighter matrix material (red star) were measured (Figures 4a,b). The reflectivity is different for the upper and lower halves of the studied area. Specifically, the upper half is darker whereas the lower half is brighter. A total of 16 nano-FTIR spectra were collected from the central part of this dark phase (Figure 4e). The spectra show a band at 1515 $cm^{-1}$ due to C═C in aromatics that gradually, from the bottom (spectrum #1, blue) to the top (spectrum #16, green), gets broader and eventually merges into the band at 1430 $cm^{-1}$, which is attributed to $CO_3^{2-}$ ions within carbonates (Figure 4e). Furthermore, the carbonate band is negatively correlated with the C—H aliphatic band near 1370−1360 $cm^{-1}$ and the sulfate band at 1175 $cm^{-1}$ as these latter two bands weaken from bottom to top as the carbonate band forms (Figure 4f). A comparison of integrated band intensities of these molecular groups clearly shows their correlations (inset in Figure 4f). The nearby matrix material (red star/spectrum) lacks individual prominent organic and sulfate peaks. Rather, this material shows a very weak and broad band centered near 1460 $cm^{-1}$, which is consistent with small amounts of carbonates. The red spectrum also shows a broader and smoother silicate band relative to the dark clast spectra, indicating abundant phyllosilicates in the matrix.

Regions-AZ3, -AZ4, and -AZ5 (Figure 2k,f,l, respectively) focus on the FGRs around chondrules in the Aguas Zarcas sample. Figure 5a presents the BSE image of Region-AZ3 where a dark-gray rim is seen around a porphyritic pyroxene chondrule. The matrix is shown as the light-gray material surrounding the chondrule and its rim. Parts b−d of Figure 5 show the optical and mechanical amplitude images as well as their combined image. A total of 10 spectra were collected from the chondrule rim in which organic peaks appear to be much weaker relative to the dark clasts previously discussed. The observed bands include a weak C═C aromatic band at 1560 $cm^{-1}$, a carbonate band at 1455 $cm^{-1}$, a sulfate band centered near 1150 $cm^{-1}$, and a silicate band centered at 1040 $cm^{-1}$. The aliphatic (C—H) band near 1370−1360 $cm^{-1}$ is completely absent in the rim. Figure 6a presents the BSE image of another FGR (Region-AZ4) that surrounds a porphyritic olivine/pyroxene chondrule that has different texture and grain size than the chondrule in Region-AZ3. The nano-FTIR spectra of the rim (red star) were measured as well as a light-gray matrix material (pink star), the overlaid optical and mechanical amplitude images of which are shown in Figure 6b,c. The infrared bands for organics, carbonates, and sulfates are absent in the nano-FTIR spectra of this rim (Figure 6d). The only prominent band is the main silicate band centered near 1030 $cm^{-1}$, shifted ∼10 $cm^{-1}$ toward lower wavenumbers. Similarly, the light-gray matrix material lacks organics, carbonates, and sulfates, although the observed silicate bands are broader than those of the rim (Figure 6e). This indicates the presence of more phyllosilicates in the matrix relative to the rim (Figure 6e). Unlike Regions-AZ1−4, Region-AZ5 surrounds a porphyritic olivine chondrule. The nano-FTIR spectra of the rim observed in Region-AZ5 show multiple bands (Figure 7), at 1127, 1040, and 980 $cm^{-1}$, which suggest contributions from anhydrous silicates. Additionally, a peak at


https://doi.org/10.1021/acsearthspacechem.1c00290
ACS Earth Space Chem. 2021, 5, 3281−3296

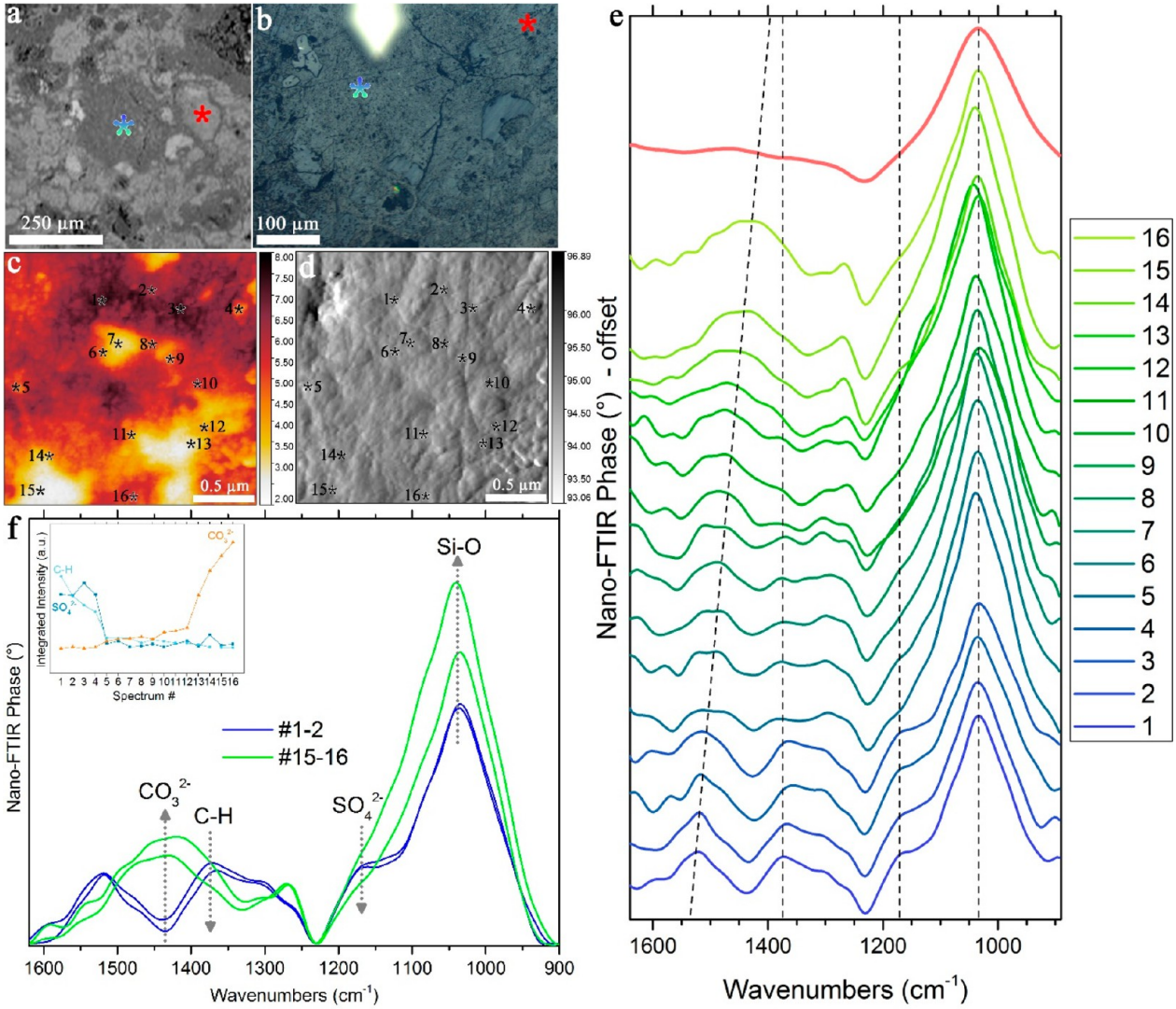


**Figure 4.** (a) BSE and (b) white-light images of Region-AZ2. Blue/green and red stars denote the locations of dark and gray phases. (c) AFM optical and (d) mechanical amplitude images indicate the spots where nano-FTIR spectra were collected underneath the blue/green star. (e) Individual nano-FTIR spectra show the evolution of the carbonate peak. The red spectrum is the average of four spectra collected from the gray material (indicated by the red star). Two spectra from both extremes as well as the inset plot (f) show the comparison and correlations of the sulfate, aliphatics, and carbonate bands.

1127 $cm^{-1}$, which is likely due to silica glass, is present in spectra #1, #2, #7, #8, and #11 but is absent in the others. Note that this band occurs at a lower wavenumber than sulfates and is better resolved.

**Nano-FTIR Spectral Results for Jbilet Winselwan.** Region-JW1 (Figure 2p) is located at the intersection of two chondrules and their respective FGRs, which are set within the matrix (Figure 8a,b). Parts c and d of Figure 8 present the optical and mechanical amplitude images of the measured area, respectively. A total of 9 spectra were collected, and nano-FTIR bands were observed at 1490, 1385, 1127, 1130, 970, 928, and 890 $cm^{-1}$ (Figure 8e). The band at 1490 $cm^{-1}$ is attributed to C—C in aromatics, and the band at 1385 $cm^{-1}$ is associated with C═O in carbonyls. The silicate region contains multiple bands, especially below 1000 $cm^{-1}$. These multiple bands are indicative of the contributions from anhydrous silicates.

Region-JW2 (Figure 2q) contains a rimmed chondrule that is not easy to discern based on the BSE image (Figure 9a,b) as it is almost indistinguishable from the matrix. Parts c and d of Figure 9 present the optical and mechanical amplitude images of the measured area, in which a total of five spectra were collected. Bands are present at 1460, 1440,1380, 1300, 1175, 1140, 1010, and 900 $cm^{-1}$. The band near 1460−1440 $cm^{-1}$ is attributed to $CO_3^{2-}$ ions within carbonates, the band at 1380 $cm^{-1}$ is attributed C═O in carbonyls, and the band at 1300 $cm^{-1}$ is attributed to C—H in aliphatics. Two weak features appear within the 1220−1100 $cm^{-1}$ region in spectra #1 and #4, which appear as a broad singlet in spectra #2 and #3, and are attributed to sulfates. The silicate band is broader than in the previously discussed spectra and is centered at 1010 $cm^{-1}$. An additional weak feature is present at 900 $cm^{-1}$, which could be attributed to olivine.

Region-JW3 (Figure 2w) is a dark phase present within the matrix material in the Jbilet Winselwan sample (Figure 10a). The optical and mechanical amplitude images as well as the overlaid amplitude image (Figure 10b−d) show that this material appears as vertical teardrop-shaped features. The nano-FTIR spectra #1, #2, and #3 exhibit a broad band centered at ∼1380 $cm^{-1}$, which might be attributed to C═O in carbonyls (Figure 9e), although this kind of broad peak is not characteristic


https://doi.org/10.1021/acsearthspacechem.1c00290
ACS Earth Space Chem. 2021, 5, 3281−3296

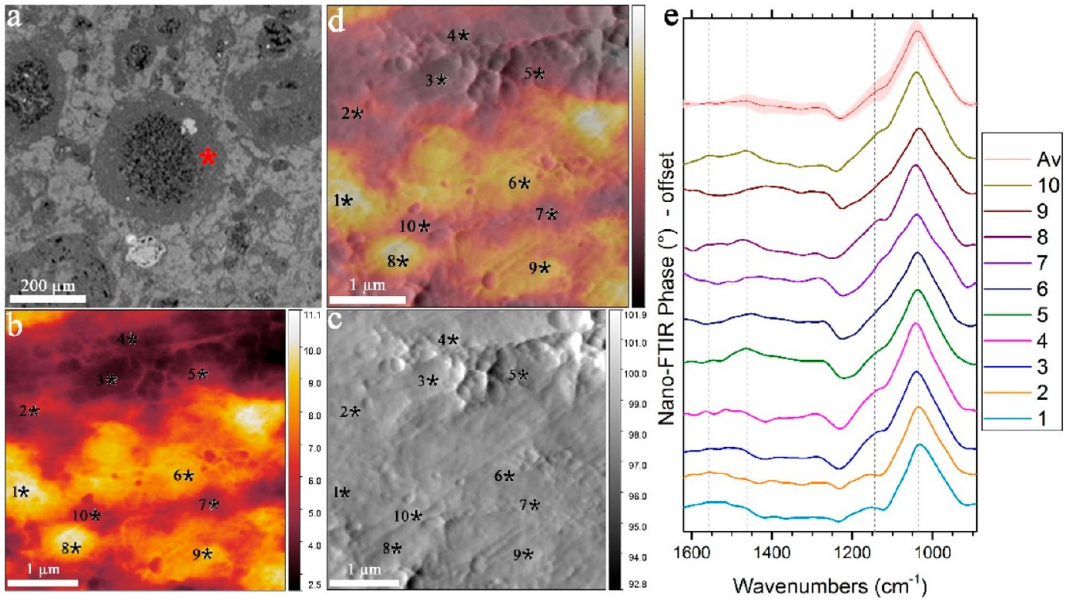


**Figure 5.** (a) BSE image of Region-AZ3. The red star denotes the studied location. AFM (b) optical, (c) mechanical, (d) amplitude, and overlaid images indicate the spots where nano-FTIR spectra were collected. Individual (e) nano-FTIR spectra show the positions of the observed bands. The average spectrum is shown in red (with the standard deviation in light red).

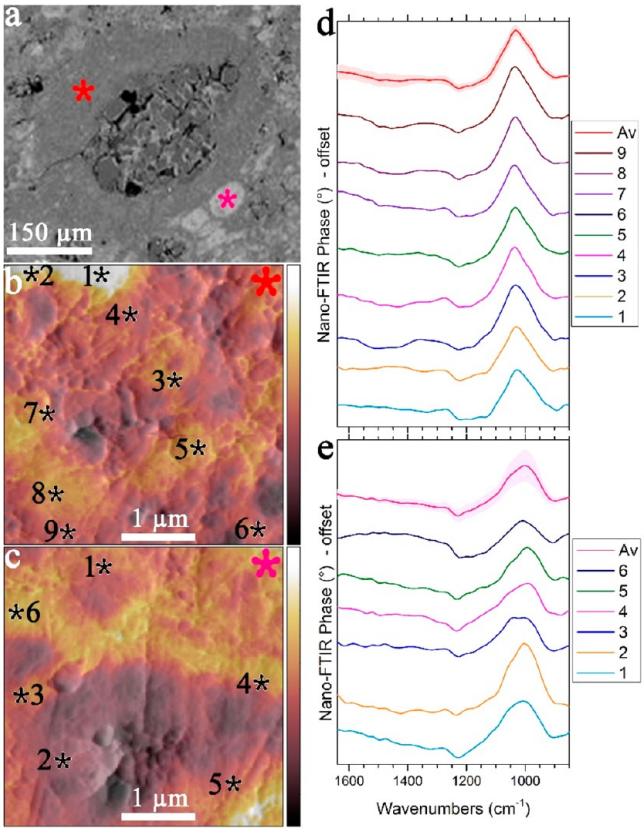


**Figure 6.** (a) BSE image of Region-AZ4. The red and pink stars denote the studied locations. (b and c) Overlaid AFM amplitude images indicate the spots where nano-FTIR spectra were collected. Individual (d and e) corresponding nano-FTIR spectra show the positions of the observed bands. The average spectra are shown in red and pink (with the standard deviation in light color).

of carbonyls. This band also looks similar to the broad band seen in the infrared spectra of powdered carbonaceous chondrites.[88,89] This band might potentially be a convolution of multiple features. This region is rather flat in spectra #4 and #5. The sharp feature at 1300 $cm^{-1}$ is observed in all of the spectra and can be attributed to C—H in aliphatics. The bands between 1200 and 1110 $cm^{-1}$ are attributed to sulfates, the spectral profile of which is different from the previously discussed bands, being quite broad and extending toward much lower wavenumbers.

Region-JW4 (Figure 2r) consists of a porphyritic olivine-pyroxene chondrule enclosed by two FGRs (Figure 11a); the outer rim can be clearly distinguished from the matrix (upper right corner) in Figure 11b. This region presents vertical vein-like patches, similar to Region-JW3, as seen in the optical, mechanical, and overlaid amplitude images (Figure 11c−e). A total of nine spectra were obtained from the inner rim, which are relatively featureless compared to the previously discussed regions. The spectra lack organic and carbonate bands, with only a silicate band being prominent at 1040 $cm^{-1}$.

Finally, Region-JW5 (Figure 2x) contains a coarse-grained porphyritic olivine-pyroxene chondrule surrounded by two FGRs (Figure 12a,b). The nano-FTIR spectra of the sampled rim, the outer rim, show no organic or carbonate bands. Similar to those of Region-JW4, the spectra only show a silicate band near 1040 $cm^{-1}$ (Figure 12e). Spectra #3 and #5, in which the silicate band is much more prominent than in spectra #1, #2, #4, and #6, also show a weak sulfate band at 1175 $cm^{-1}$.

Raman spectroscopy is complementary to infrared spectroscopy and is highly sensitive to many molecular functional groups including carbon-rich structures such as aromatic moieties in meteorites. The Raman spectra of various FGRs and dark clasts present in Aguas Zarcas and Jbilet Winselwan exhibit well-developed first-order carbon bands at ∼1370 and 1581 $cm^{-1}$ (Figure 13). These carbon bands are referred to as D and G bands and are due to disordered sp3 and graphitic-like sp2 carbon bonds, respectively.[90−92] Raman spectroscopic investigation of meteoritic carbon is particularly useful as the thermal metamorphic grade/history of carbonaceous chondrites can be roughly estimated through the spectral properties of poly-aromatic structures in meteorites. By using full-width-half-


https://doi.org/10.1021/acsearthspacechem.1c00290
ACS Earth Space Chem. 2021, 5, 3281−3296

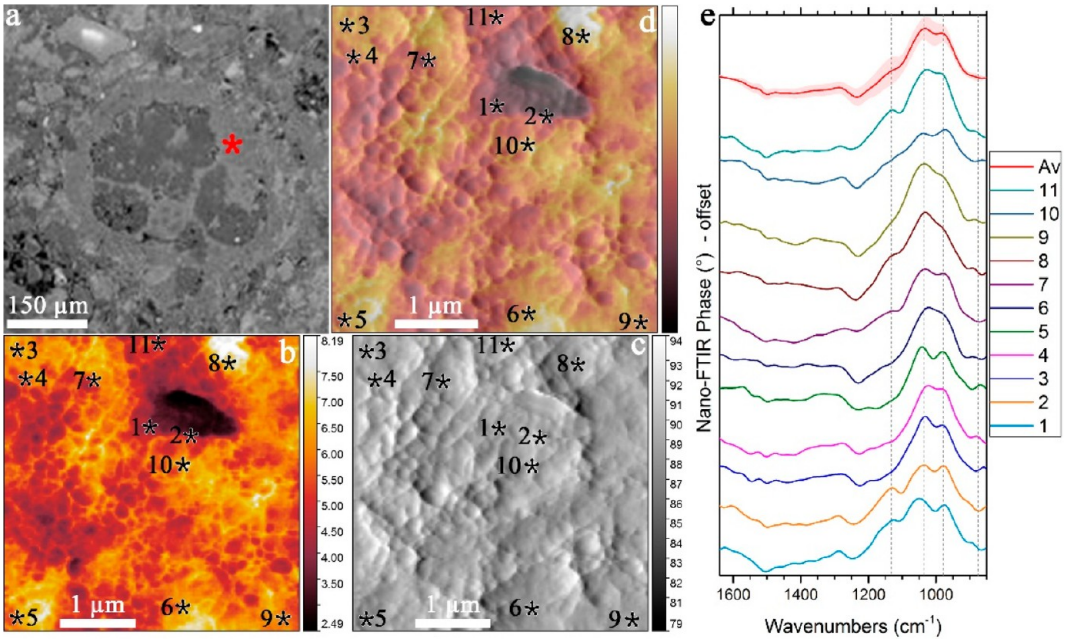


**Figure 7.** (a) BSE image of Region-AZ5. The red star denotes the studied location. AFM (b) optical, (c) mechanical, (d) amplitude, and overlaid images indicate the spots where nano-FTIR spectra were collected. Individual (e) nano-FTIR spectra show the positions of the observed bands. The average spectrum is shown in red (with the standard deviation in light red).

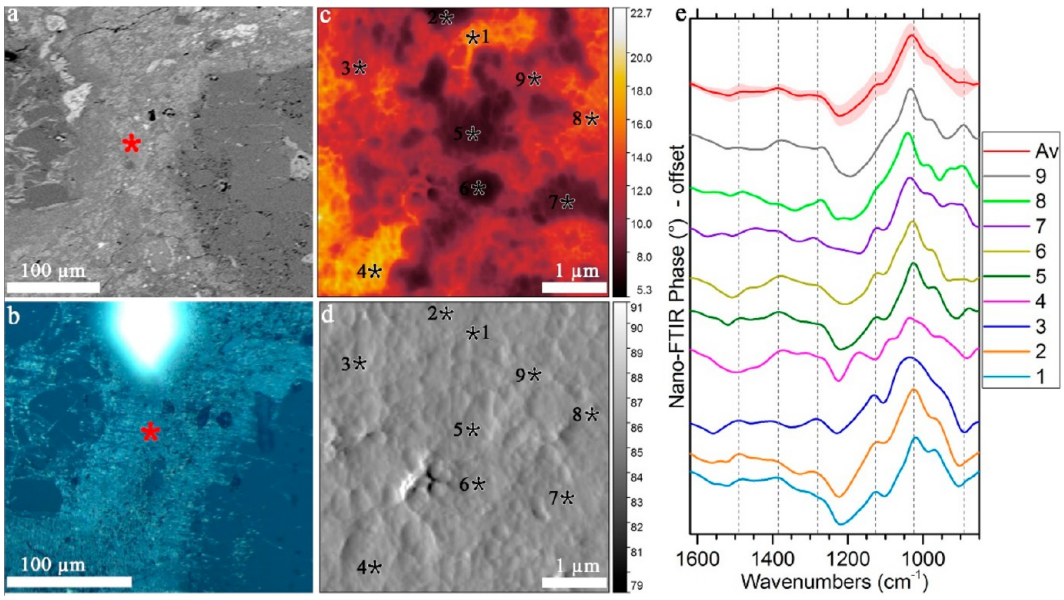


**Figure 8.** (a) BSE and (b) white-light images of Region-JW1. The red star denotes the studied location. AFM (c) optical and (d) mechanical images indicate the spots where nano-FTIR spectra were collected. Individual (e) nano-FTIR spectra show the positions of the observed bands. The average spectrum is shown in red (with the standard deviation in light red).

maxima and position of the G band, and expressions reported by Cody et al.[93] and Schmidt et al.,[94] we calculated the peak metamorphic temperatures of Aguas Zarcas and Jbilet Winselwan. The calculation for FGRs and dark clasts yields 68−75 °C for the two CM2 chondrites if the expression by Schmidt et al.[94] was used (Figure 13). The expression by Cody et al.[93] yields higher metamorphic temperatures (146−175 °C).

## ■ DISCUSSION

Many groups have previously identified organic matter within the matrices of carbonaceous chondrites. CM chondrites contain, on average, ∼2 wt % of bulk carbon, about half of which is in the insoluble organic matter content.[96−98] A diversity of organics has been found to be distributed within the matrices of CM chondrites. In Murchison, organic matter appears to be associated with and interspersed within Mg-rich phyllosilicates at the nanometer scale.[99] Paris (CM2), one of the least altered CM chondrites,[13] has a matrix that contains abundant aliphatic-type organics.[100] A comparison of Paris with Murchison using X-ray absorption near-edge structure (XANES) and scanning transmission X-ray microscopy (STXM) indicated that the former meteorite contains two distinct populations of organic compounds (individual grains and diffuse organic matter) and has a higher aliphatic/aromatic carbon ratio.[101] Using


https://doi.org/10.1021/acsearthspacechem.1c00290
ACS Earth Space Chem. 2021, 5, 3281−3296

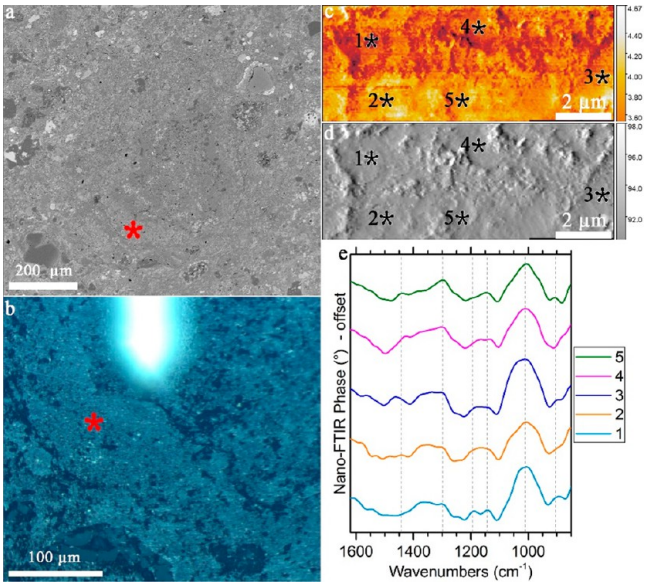


**Figure 9.** (a) BSE and (b) white-light images of Region-JW2. The red star denotes the studied location. AFM (c) optical and (d) mechanical images indicate the spots where nano-FTIR spectra were collected. Individual (e) nano-FTIR spectra show the positions of the observed bands. The average spectrum is shown in red (with the standard deviation in light red).

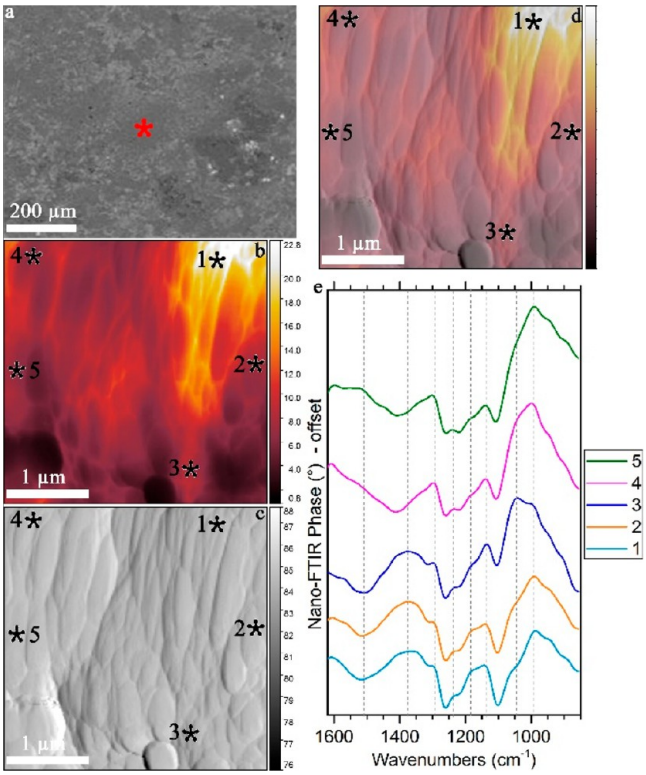


**Figure 10.** (a) BSE image of Region-JW3. Red star denotes the studied location. AFM (b) optical and (c) mechanical amplitude images as well as (d) overlaid image indicate the spots whose nano-FTIR spectra were collected. Individual (e) nano-FTIR spectra present positions of observed bands.

synchrotron-based infrared spectro-microtomography, Yesiltas et al.[88] identified aliphatics and aromatics within a matrix grain of Murchison *in situ* in three-dimensional space. In this current work, we have identified organic matter within the matrices of two CM2 chondrites (Aguas Zarcas and Jbilet Winselwan). Our observations (i.e., identification of organics and their types) are in good agreement with previous identifications of organics in CM chondrites. In addition, we have identified organics embedded within some of the FGRs in Aguas Zarcas. To our knowledge, this work is the first to identify organic matter within FGRs.

The origin of organic matter in carbonaceous chondrites is still not fully constrained. A considerable amount of work is being done to better understand and constrain the formation regions and pathways of organics, though whether organics are nebular and formed prior to accretion,[102−105,96,106−109] interstellar,[110−114] or solar and formed on the parent body postaccretion[115−120] is still an outstanding question. Alexander et al.[96,121] assessed both possibilities in comprehensive reviews. Much of the work toward understanding the origin and nature of organic matter in chondrites is being done on the insoluble organic portion that is extracted through chemical reactions. XANES, STXM, TEM, micro-FTIR, and Raman spectroscopies are among the analytical techniques used for investigating organic content of chondrites at the micrometer scale, though chondritic materials such as matrix and rims are composed of submicron particles. Nano-FTIR spectroscopy is a powerful and nondestructive analytical technique for the investigation of samples including carbonaceous chondrites and their fine-grained components. It offers a spatial resolution of ∼20 nm.[54,77−80] This technique does not require powdered or chemically processed samples nor does it alter samples in any way, thus fully preserving the petrographic context, and it is independent of the optical diffraction limit. It was recently used to detect nanoscale carbonyl compounds in a primitive CO3 chondrite.[80] In this current work, nano-FTIR spectra of FGRs and dark clasts show that they are chemically heterogeneous at a submicron scale, and some rims contain organic molecules in addition to hydrated minerals. It is currently unknown whether the organics observed in the Aguas Zarcas FGRs are nebular in origin; however, it is plausible that organics could have formed in the solar nebula *via* surface polymerization in the icy mantles of dust grains, mixed with dust, and became incorporated—along with the FGRs—around the chondrules before undergoing planetary thermal processing. In this case, the organics identified in our samples would predate the postaccretionary processes. Alternatively, fluid flow during aqueous alteration on the parent bodies may have deposited organic matter into the pores of FGRs postaccretion, even though the FGRs generally have significantly lower porosity than matrix.

The Aguas Zarcas and Jbilet Winselwan meteorite samples contain numerous chondrules surrounded by FGRs that are texturally distinct from the enclosed objects. FGRs almost always continuously enclose the chondrules. This is interpreted to suggest that brecciation was limited after the chondrules were surrounded, otherwise more chondrules would have discontinuous rims (e.g., ref 25). This is not the case in both of the CM2 chondrites we studied in this work. Specifically, the surrounding FGRs in the Aguas Zarcas sample were found to be quite distinct from the enclosed objects. In the BSE images of Aguas Zarcas, FGRs appear relatively darker than the adjacent matrix, which appears light gray, indicating a lower atomic number density relative to the matrix. Our EDS data show that the FGRs in Aguas Zarcas have nearly identical compositions regardless of the enclosed chondrule (Figure S1). This similarity could indicate sampling from the same reservoir.[5,122] The FGRs and


https://doi.org/10.1021/acsearthspacechem.1c00290
ACS Earth Space Chem. 2021, 5, 3281−3296

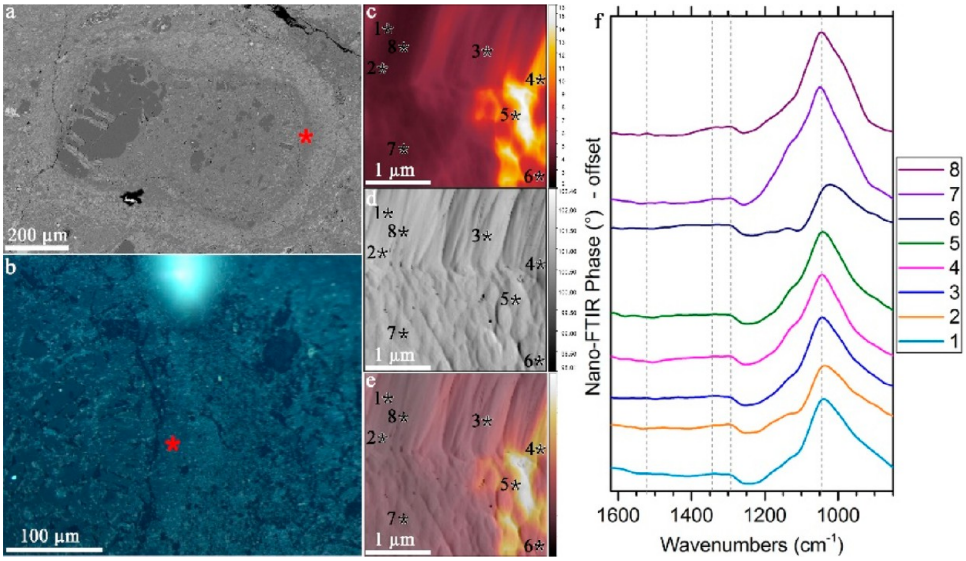


**Figure 11.** (a) BSE and (b) white-light images of Region-JW4. Red star denotes the studied location. AFM (c) optical and (d) mechanical amplitude images as well as overlaid (e) image indicate the spots where nano-FTIR spectra were collected. Individual (f) nano-FTIR spectra present positions of the observed bands.

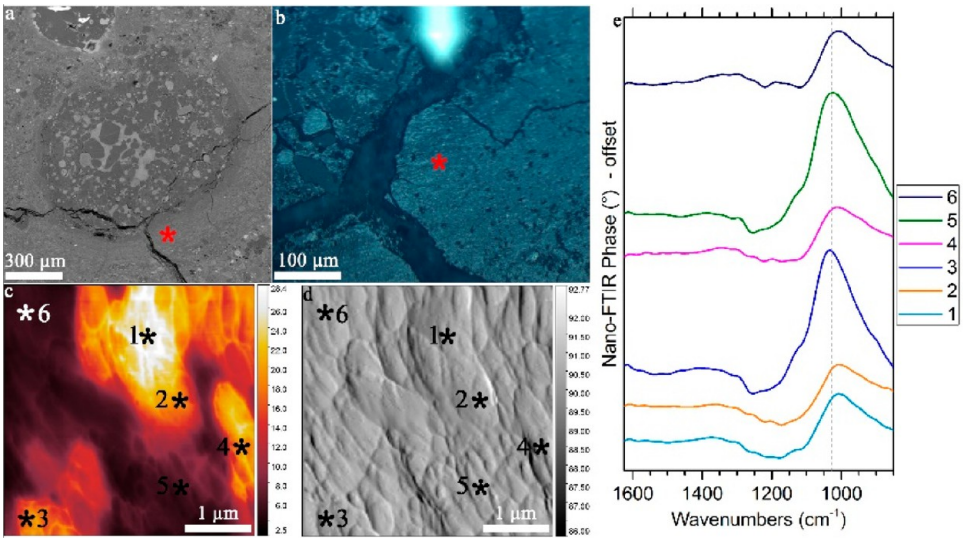


**Figure 12.** (a) BSE and (b) white-light images of Region-JW5. Red star denotes the studied location. AFM (c) optical and (d) mechanical amplitude images indicate the spots where nano-FTIR spectra were collected. Individual (e) nano-FTIR spectra present positions of the observed bands.

matrix are compositionally very similar. This observation is consistent with previous work on CM chondrites (e.g., ref 1). In Jbilet Winselwan, the FGRs appear somewhat similar in atomic number density to the matrix. In some cases, it proved difficult to distinguish the FGR from the matrix because the interface between the two materials is not sharp. This difference between the Aguas Zarcas and Jbilet Winselwan samples likely reflects significant impact-brecciation in the case of the latter meteorite, which would have caused shock and dehydration/decomposition of the hydrated phases (e.g., ref 65).

Severe thermal metamorphism can potentially cause FGRs and enclosed chondrules to recrystallize and coarsen. In that case, it would be difficult to differentiate chondrules from rims. As Aguas Zarcas contains numerous well-defined continuous FGRs around different types of chondrules, thermal metamorphism was not severe. Jbilet Winselwan also shows many FGRs around chondrules, although the "spongy" texture of matrix and dehydrated lithologies confirm that this CM2 chondrite was heated, probably not through long-duration thermal metamorphism but rather through significant but short-duration heating. Even though the FGRs in this sample are not as ubiquitous as those in Aguas Zarcas, their presence indicates that such a short duration heating did not result in the merging of the FGRs and enclosed chondrules and the formation of a larger chondrule. In addition, both chondrites were found to contain abundant organic matter, such as aromatics, aliphatics, and carbonyls.[52] These organic materials would have decomposed even under mild thermal metamorphism,[44] providing further evidence that both Aguas Zarcas and Jbilet Winselwan experienced minimal thermal metamorphism, although Jbilet Winselwan is relatively more metamorphosed.

The thicknesses of the FGRs vary between 5 and 200 $\mu$m in both meteorites, and rim thickness increases with the size of the surrounded object, indicating a positive correlation (Figure S2).


https://doi.org/10.1021/acsearthspacechem.1c00290
ACS Earth Space Chem. 2021, 5, 3281−3296

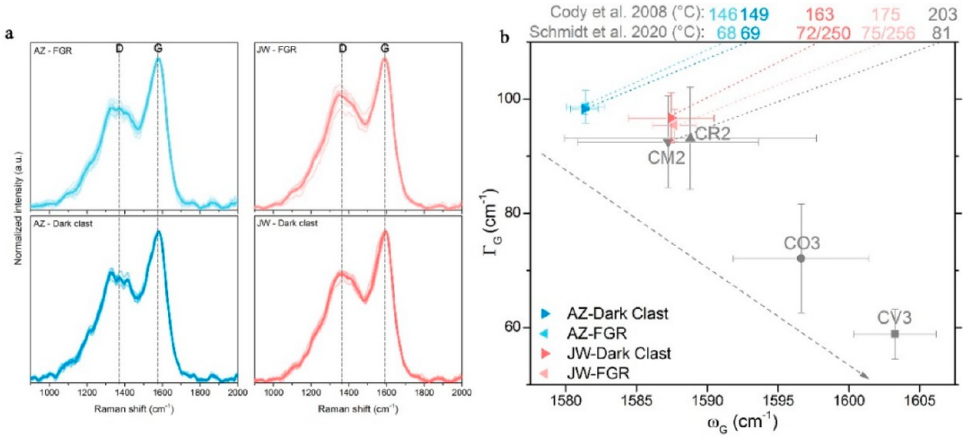


**Figure 13.** (a) Individual (light color) and average (dark color) Raman spectra of organic content within dark clasts and FGRs identified in Aguas Zarcas and Jbilet Winselwan as well as (b) their corresponding G-band parameters compared with other carbonaceous chondrite groups. The dashed gray arrow in (b) indicates increasing thermal metamorphism. Estimated peak metamorphic temperatures are shown on top of (b). CV3 and CO3 data are from Yesiltas et al.[82] CM2 and CR2 data are from Busemann et al.[95]

This relationship seems to be independent of the enclosed chondrule type, i.e., the texture, chondrule type, or grain size appear to have no effect on the rim thickness or its correlation with the chondrule size. In addition, some FGRs contain anhydrous silicates even though most FGRs are composed mainly of hydrated phases. Some chondrules in Jbilet Winselwan were found to contain double and sometimes even triple rims, such as those shown in Figure 2o,u. In the case of double rims, the inner rim is usually darker than the outer rim, which, in some cases, is itself indistinguishable from the matrix. These evidences suggest that the aqueous alteration of the FGRs was not severe and did not proceed to completion.[28,31]

The FGRs in CM2 chondrites could have formed in the parent body through a variety of processes. *In situ* aqueous alteration of chondrules on the parent body, which would lead to a more homogeneous degree of phase alteration, is one potential formation pathway.[28,45,123−126] Regolith gardening in the parent body has also been proposed as a mechanism of FGR formation.[24,43] Regolith gardening is a disruptive process resulting in FRG fragmentation and rims with homogeneous elemental compositions and similar bulk compositions in CM chondrites.[25,28] However, the Aguas Zarcas and Jbilet Winselwan FRGs exhibit an absence of homogeneous phase alteration and rim fragmentation. They exhibit no rim fragmentation, the majority of rims are completely continuous and surround chondrules. They also lack chondrule replacement by rims; most of the FGRs present very similar chemical compositions regardless of the enclosed chondrule mineralogy. These observations do not support the parent body alteration or regolith gardening formation pathways. On the contrary, the positive correlation between rim thickness with chondrule diameter, similar FGR compositions that are independent of surrounded chondrules, and presence of less aqueously altered rims support nebular origin of FGRs (e.g., ref 5).

Brecciated carbonaceous chondrites, like those investigated here, contain different types of clasts and lithologies including those rich in organic matter and hydrated phases. Some of the clasts could be exogenous, i.e., foreign to the host meteorite. These clasts and lithologies could even potentially originate from a previously unsampled/unknown body. Thus, further comparison of clasts and rims could help better constrain their origin and formation/evolution histories. Furthermore, thermal metamorphism induces irreversible transformations on the carbon structures. Raman spectroscopy is highly sensitive to aromatic moieties, and the thermal metamorphic grade/history of carbonaceous materials can be deduced *via* Raman spectral investigation of polyaromatic structures in meteorites. Using expressions by Cody et al.[93] and Schmidt et al.,[94] we estimated the peak metamorphic temperatures for FGRs and dark clasts. In this case, the comparison of the Raman spectral parameters of the aromatics in both FGRs and dark clasts of Aguas Zarcas and Jbilet Winselwan shows that the spectral parameters of FGRs and dark clasts plot very close to each other, indicating similar thermal metamorphic history for these two types of materials (Figure 13). The thermal metamorphism appears to have not caused significant modifications on their respective aromatic carbon structures, and they are consistent with being petrologic type 2 chondrites. Jbilet Winselwan is relatively more heated than Aguas Zarcas, which is in agreement with its observed textures and composition. The peak metamorphic temperatures of Aguas Zarcas and Jbilet Winselwan, calculated following Schmidt et al.,[94] are also similar (68−69 ± 3 vs 72−75 ± 6 °C, respectively) (Figure 13). Because the latter meteorite experienced short-term flash heating, it must have experienced relatively elevated temperatures. Using equations by Schmidt et al.,[94] its "elevated" metamorphic temperature was calculated to be 253 ± 3 °C. Note that using the expression by Cody et al.[93] yields higher temperatures for the same G band parameters. The similar metamorphic temperatures of the aromatics within the FGRs and dark clasts may indicate homogeneity in the polyaromatic structures in the two material types. At the same time, this may indicate that the polyaromatic-type organics in the FGRs and dark clasts may have originated from similar precursors, accreted at similar times, and/or experienced similar processes. Aromatic carbon can be processed by UV irradiation in the interstellar medium. Indeed, abundant aromatic carbon has been identified in the interstellar medium,[127,128] where UV irradiation causes a loss of $sp^3$ carbon and modifies amorphous aromatic carbon toward a more graphitic structure.[129] Thus, the formation/processing of aromatics in the interstellar medium cannot be ruled out. More detailed analyses are required to unambiguously determine the origin of the organics within the FGRs and dark clasts in carbonaceous chondrites.


https://doi.org/10.1021/acsearthspacechem.1c00290
ACS Earth Space Chem. 2021, 5, 3281−3296

## ■ CONCLUSIONS

Focusing on two CM2 chondrites, Aguas Zarcas and Jbilet Winselwan, we obtained BSE images showing the presence of several dark clasts and numerous continuous well-defined FGRs around chondrules. Chondrule diameters are found to be positively correlated with rim thickness. Notably, the observed FGRs show an absence of homogeneous phase alteration and fragmentation and, thus, appear to have experienced minimal brecciation after the chondrules were surrounded. The FGRs have almost identical chemical compositions, and this is independent of the composition of enclosed chondrules. The FGRs and matrix are also compositionally very similar, although they exhibit different textures and grain sizes. These evidence suggest that the FGRs may have a nebular origin. Owing to its superior spatial resolution and wavelength independent and nondestructive nature, nano-FTIR spectra of the dark clasts and FGRs showed that they are chemically heterogeneous at a submicron scale. The dark clasts and FGRs in Aguas Zarcas are composed of organics (i.e., aliphatics, aromatics, and carbonyls) as well as secondary alteration minerals (i.e., phyllosilicates, carbonates, and sulfates) and primary silicates. The presence of organics within the FGRs may indicate that the organics may have formed in the solar nebula and incorporated around the chondrules along with the FGRs before undergoing planetary thermal processing. Organics may have alternatively deposited into the pores of FGRs due to fluid flow during aqueous alteration on the parent bodies. The transformation of organics to carbonates is also observed within a matter of few microns in a dark clast of Aguas Zarcas, indicating highly heterogeneous composition. Moreover, the FGRs and dark clasts show polyaromatic structures with similar thermal metamorphic temperatures. This may indicate that the organics in the FGRs and dark clasts originated from similar precursors, accreted at similar times, and/or experienced similar processes. Our observations suggest that both Aguas Zarcas and Jbilet Winselwan experienced minimal thermal metamorphism, although the latter is relatively more metamorphosed and exhibits spongy matrix textures, which could be the result of a short-duration heating event such as impact heating. This process may also have caused a shock and dehydration/decomposition of the hydrated phases. More detailed analyses are now required to unambiguously determine the origin of FGRs and dark clasts in carbonaceous chondrites.

## ■ ASSOCIATED CONTENT

### Supporting Information

The Supporting Information is available free of charge at https://pubs.acs.org/doi/10.1021/acsearthspacechem.1c00290.

Figures of SEM-EDS data for FGRs and matrix and comparison of rim thickness with enclosed chondrule diameter (PDF)

## ■ AUTHOR INFORMATION


### Corresponding Author

**Mehmet Yesiltas** − *Faculty of Aeronautics and Space Sciences, Kirklareli University, Kirklareli 39100, Turkey;* orcid.org/0000-0002-1521-0460; Email: myesiltas@knights.ucf.edu

### Authors

**Timothy D. Glotch** − *Department of Geosciences, Stony Brook University, Stony Brook, New York 11794, United States*

**Melike Kaya** − *Institute of Acceleration Technologies, Ankara University, Ankara 06830, Turkey; Turkish Accelerator and Radiation Laboratory (TARLA), Ankara 06830, Turkey*

Complete contact information is available at: https://pubs.acs.org/10.1021/acsearthspacechem.1c00290


### Author Contributions

The manuscript was written through contributions of all authors. All authors have given approval to the final version of the manuscript.


### Funding

TUBITAK NASA-SSERVI


### Notes

The authors declare no competing financial interest.

## ■ ACKNOWLEDGMENTS

This work was supported by TUBITAK (PI: M.Y., project numbers 119N207 and 120Y115) and RISE2 node of NASA-SSERVI (PI: T.D.G.). M.K. acknowledges the TARLA project, founded by the Ministry of Development in Turkey (project code: DPT2006K12-827).

## ■ ABBREVIATIONS USED

nano-FTIR, nanoscale Fourier-transform infrared spectroscopy; AFM, atomic force microscope; FGR, fine-grained rim; SEM, scanning electron microscopy; BSE, backscattered electron

## ■ REFERENCES


(1) Zolensky, M.; Barrett, R.; Browning, L. Mineralogy and composition of matrix and chondrule rims in carbonaceous chondrites. *Geochim. Cosmochim. Acta* **1993**, *57* (13), 3123−3148.

(2) Brearley, A. J.; Jones, R. H. Chapter 3: Chondritic Meteorites. *Planetary Materials, volume 36 of Reviews in Mineralogy*; Mineralogical Society of America: Washington, DC, 1998; 3.01−3.398.

(3) Barber, D. J. Matrix phyllosilicates and associated minerals in C2M carbonaceous chondrites. *Geochim. Cosmochim. Acta* **1981**, *45* (6), 945−970.

(4) Tomeoka, K.; Buseck, P. R. Indicators of aqueous alteration in CM carbonaceous chondrites: Microtextures of a layered mineral containing Fe, S, O and Ni. *Geochim. Cosmochim. Acta* **1985**, *49* (10), 2149−2163.

(5) Metzler, K.; Bischoff, A.; Stöffler, D. Accretionary dust mantles in CM chondrites: Evidence for solar nebula processes. *Geochim. Cosmochim. Acta* **1992**, *56* (7), 2873−2897.

(6) Browning, L. B.; McSween Jr, H. Y.; Zolensky, M. E. Correlated alteration effects in CM carbonaceous chondrites. *Geochim. Cosmochim. Acta* **1996**, *60* (14), 2621−2633.

(7) Zolensky, M. E.; Mittlefehldt, D. W.; Lipschutz, M. E.; Wang, M. S.; Clayton, R. N.; Mayeda, T. K.; Grady, M. M.; Pillinger, C.; David, B. CM chondrites exhibit the complete petrologic range from type 2 to 1. *Geochim. Cosmochim. Acta* **1997**, *61* (23), 5099−5115.

(8) Rubin, A. E.; Trigo-Rodríguez, J. M.; Huber, H.; Wasson, J. T. Progressive aqueous alteration of CM carbonaceous chondrites. *Geochim. Cosmochim. Acta* **2007**, *71* (9), 2361−2382.

(9) Yabuta, H.; Williams, L. B.; Cody, G. D.; Alexander, C.M.O'D.; Pizzarello, S. The insoluble carbonaceous material of CM chondrites: A possible source of discrete organic compounds under hydrothermal conditions. *Meteorit. Planet. Sci.* **2007**, *42* (1), 37−48.

(10) Cloutis, E. A.; Hudon, P.; Hiroi, T.; Gaffey, M. J.; Mann, P. Spectral reflectance properties of carbonaceous chondrites: 2. CM chondrites. *Icarus* **2011**, *216* (1), 309−346.

(11) Kimura, M.; Grossman, J. N.; Weisberg, M. K. Fe-Ni metal and sulfide minerals in CM chondrites: An indicator for thermal history. *Meteoritics & Planetary Science* **2011**, *46* (3), 431−442.

(12) Brearley, A. J. Nebular vs parent body processing of chondritic meteorites. In *Meteorites, comets and planets*, 2nd ed.; Davis, A. M., Ed.; Elsevier: Cambridge, UK, 2013; pp 309−334.
(13) Hewins, R. H.; Bourot-Denise, M.; Zanda, B.; Leroux, H.; Barrat, J. A.; Humayun, M.; Göpel, C.; Greenwood, R. C.; Franchi, I. A.; Pont, S.; Lorand, J. P.; et al. The Paris meteorite, the least altered CM chondrite so far. *Geochim. Cosmochim. Acta* **2014**, *124*, 190−222.
(14) Tonui, E.; Zolensky, M.; Hiroi, T.; Nakamura, T.; Lipschutz, M. E.; Wang, M. S.; Okudaira, K. Petrographic, chemical and spectroscopic evidence for thermal metamorphism in carbonaceous chondrites I: CI and CM chondrites. *Geochim. Cosmochim. Acta* **2014**, *126*, 284−306.
(15) Verdier-Paoletti, M. J.; Marrocchi, Y.; Avice, G.; Roskosz, M.; Gurenko, A.; Gounelle, M. Oxygen isotope constraints on the alteration temperatures of CM chondrites. *Earth Planet. Sci. Lett.* **2017**, *458*, 273−281.
(16) Piani, L.; Yurimoto, H.; Remusat, L. A dual origin for water in carbonaceous asteroids revealed by CM chondrites. *Nature astronomy* **2018**, *2* (4), 317−323.
(17) Leitner, J.; Metzler, K.; Vollmer, C.; Floss, C.; Haenecour, P.; Kodolányi, J.; Harries, D.; Hoppe, P. The presolar grain inventory of fine-grained chondrule rims in the Mighei-type (CM) chondrites. *Meteorit. Planet. Sci.* **2020**, *55* (6), 1176−1206.
(18) King, A. J.; Schofield, P. F.; Russell, S. S. Thermal alteration of CM carbonaceous chondrites: Mineralogical changes and metamorphic temperatures. *Geochim. Cosmochim. Acta* **2021**, *298*, 167−190.
(19) Nittler, L. R.; Alexander, C. M. O. D.; Patzer, A.; Verdier-Paoletti, M. J. Presolar stardust in highly pristine CM chondrites Asuka 12169 and Asuka 12236. *Meteorit. Planet. Sci.* **2021**, *56* (2), 260−276.
(20) Velbel, M. A.; Zolensky, M. E. Thermal metamorphism of CM chondrites: A dehydroxylation-based peak-temperature thermometer and implications for sample return from asteroids Ryugu and Bennu. *Meteorit. Planet. Sci.* **2021**, *56* (3), 546−585.
(21) Brearley, A. J. Matrix and fine-grained rims in the unequilibrated CO3 chondrite, ALHA77307: Origins and evidence for diverse, primitive nebular dust components. *Geochim. Cosmochim. Acta* **1993**, *57* (7), 1521−1550.
(22) Brearley, A. J. Nanophase iron carbides in fine-grained rims in CM2 carbonaceous chondrites: Formation of organic material by Fischer−Tropsch catalysis in the solar nebula. *Meteorit. Planet. Sci.* **2021**, *56* (1), 108−126.
(23) Lauretta, D. S.; Hua, X.; Buseck, P. R. Mineralogy of fine-grained rims in the ALH 81002 CM chondrite. *Geochim. Cosmochim. Acta* **2000**, *64* (19), 3263−3273.
(24) Tomeoka, K.; Tanimura, I. Phyllosilicate-rich chondrule rims in the Vigarano CV3 chondrite: Evidence for parent-body processes. *Geochim. Cosmochim. Acta* **2000**, *64* (11), 1971−1988.
(25) Hua, X.; Wang, J.; Buseck, P. R. Fine-grained rims in the Allan Hills 81002 and Lewis Cliff 90500 CM2 meteorites: Their origin and modification. *Meteorit. Planet. Sci.* **2002**, *37* (2), 229−244.
(26) Ciesla, F. J.; Lauretta, D. S.; Cohen, B. A.; Hood, L. L. A nebular origin for chondritic fine-grained phyllosilicates. *Science* **2003**, *299* (5606), 549−552.
(27) Zega, T. J.; Buseck, P. R. Fine-grained-rim mineralogy of the Cold Bokkeveld CM chondrite. *Geochim. Cosmochim. Acta* **2003**, *67* (9), 1711−1721.
(28) Greshake, A.; Krot, A. N.; Flynn, G. J.; Keil, K. Fine-grained dust rims in the Tagish Lake carbonaceous chondrite: Evidence for parent body alteration. *Meteoritics & Planetary Science* **2005**, *40* (9−10), 1413−1431.
(29) Huss, G. R., Alexander, C. M. O'D., Palme, H., Bland, P. A.; Wasson, J. T. Genetic relationships between chondrules, fine-grained rims, and interchondrule matrix. *Chondrites and the Protoplanetary Disk, ASP Conference Series, Vol. 341*, Kaua'i, Hawaii, November 8−11, 2004; Astronomical Society of the Pacific, 2005; p 701.
(30) Leitner, J.; Vollmer, C.; Floss, C.; Zipfel, J.; Hoppe, P. Ancient stardust in fine-grained chondrule dust rims from carbonaceous chondrites. *Earth Planet. Sci. Lett.* **2016**, *434*, 117−128.
(31) Zanetta, P. M.; Leroux, H.; Le Guillou, C.; Zanda, B.; Hewins, R. H. Nebular thermal processing of accretionary fine-grained rims in the Paris CM chondrite. *Geochim. Cosmochim. Acta* **2021**, *295*, 135−154.
(32) Bischoff, A. Aqueous alteration of carbonaceous chondrites: Evidence for preaccretionary alteration—A review. *Meteorit. Planet. Sci.* **1998**, *33* (5), 1113−1122.
(33) King, T. V. V.; King, E. A. Accretionary dark rims in unequilibrated chondrites. *Icarus* **1981**, *48*, 460−472.
(34) Scott, E. R. Classification, metamorphism, and brecciation of type 3 chondrites from Antarctica. *Smithsonian Contributions to the Earth Sciences* **1984**, *26*, 73−94.
(35) Rubin, A. E. Coarse-grained chondrule rims in type 3 chondrites. *Geochim. Cosmochim. Acta* **1984**, *48* (9), 1779−1789.
(36) MacPherson, G. J.; Hashimoto, A.; Grossman, L. Accretionary rims on inclusions in the Allende meteorite. *Geochim. Cosmochim. Acta* **1985**, *49* (11), 2267−2279.
(37) Rubin, A. E.; Wasson, J. T. Chondrules, matrix and coarse-grained chondrule rims in the Allende meteorite: Origin, interrelationships and possible precursor components. *Geochim. Cosmochim. Acta* **1987**, *51* (7), 1923−1937.
(38) Brearley, A. J.; Geiger, T. Mineralogical and chemical studies bearing on the origin of accretionary rims in the Murchison CM2 carbonaceous chondrite. *Meteoritics* **1991**, *26*, 323.
(39) Tomeoka, K.; Hatakeyama, K.; Nakamura, T.; Takeda, H. Evidence for Pre-accretionary aqueous alteration in the Yamato-793321 CM carbonaceous chondrite. *Antarctic Meteorites XVI* **1991**, *16*, 37−39.
(40) Nakamura, T.; Tomeoka, K.; Takeda, H. Mineralogy of chondrule rims in the Yamato-791198 CM chondrite: Comparison to Murchison. *Antarctic Meteorites XVI* **1991**, *16*, 40−41.
(41) Hua, X.; Zinner, E. K.; Buseck, P. R. Petrography and chemistry of fine-grained dark rims in the Mokoia CV3 chondrite: Evidence for an accretionary origin. *Geochim. Cosmochim. Acta* **1996**, *60* (21), 4265−4274.
(42) Chizmadia, L. J.; Brearley, A. J. Mineralogy, aqueous alteration, and primitive textural characteristics of fine-grained rims in the Y-791198 CM2 carbonaceous chondrite: TEM observations and comparison to ALHA81002. *Geochim. Cosmochim. Acta* **2008**, *72* (2), 602−625.
(43) Sears, D. W.; Benoit, P. H.; Jie, L. Two chondrule groups each with distinctive rims in Murchison recognized by cathodoluminescence. *Meteoritics* **1993**, *28* (5), 669−675.
(44) Hanowski, N. P.; Brearley, A. J. Aqueous alteration of chondrules in the CM carbonaceous chondrite, Allan Hills 81002: Implications for parent body alteration. *Geochim. Cosmochim. Acta* **2001**, *65* (3), 495−518.
(45) Trigo-Rodriguez, J. M.; Rubin, A. E.; Wasson, J. T. Non-nebular origin of dark mantles around chondrules and inclusions in CM chondrites. *Geochim. Cosmochim. Acta* **2006**, *70* (5), 1271−1290.
(46) Takayama, A.; Tomeoka, K. Fine-grained rims surrounding chondrules in the Tagish Lake carbonaceous chondrite: Verification of their formation through parent-body processes. *Geochim. Cosmochim. Acta* **2012**, *98*, 1−18.
(47) Brearley, A. J.; Hanowski, N. P.; Whalen, J. F. Fine-grained rims in CM carbonaceous chondrites: A comparison of rims in Murchison and ALH 81002. *Lunar Planet. Sci.* **1999**, 1460.
(48) Zolensky, M. E.; Weisberg, M. K.; Buchanan, P. C.; Prinz, M.; Reid, A.; Barrett, R. A. Mineralogy of Dark Clasts in CT Chondrites, Encrites and Howardites. *Abstracts of the Lunar and Planetary Science Conference* **1992**, *23*, 1587.
(49) Zolensky, M. E., Ohsumi, K., Briani, G., Gounelle, M., Mikouchi, T., Satake, W., Kurihara, T., Weisberg, M. K.; Le, L. Searching for chips of Kuiper Belt objects in meteorites. *40th Lunar and Planetary Science Conference*, The Woodlands, TX, March 23−27, 2009
(50) Buchanan, P. C.; Zolensky, M. E.; Reid, A. M. Carbonaceous chondrite clasts in the howardites Bholghati and EET87513. *Meteoritics* **1993**, *28* (5), 659−669.
(51) Kebukawa, Y.; Zolensky, M. E.; Chan, Q. H.; Nagao, K.; Kilcoyne, A. D.; Bodnar, R. J.; Farley, C.; Rahman, Z.; Le, L.; Cody, G. D. Characterization of carbonaceous matter in xenolithic clasts from the

Sharps (H3. 4) meteorite: Constraints on the origin and thermal processing. *Geochim. Cosmochim. Acta* **2017**, *196*, 74−101.
(52) Kebukawa, Y.; Zolensly, M.; Mathurin, J.; Dartois, E.; Engrand, C.; Duprat, J.; Deniset-Besseau, A.; Dazzi, A.; Fries, M.; Ohigashi, T.; Wakabayashi, D. Organic matter in the Aguas Zarcas (CM2) meteorite: high abundance of aliphatic carbon in metal-rich lithology. *51st Lunar and Planetary Science Conference*, The Woodlands, Texas, March 16−20, 2020; Vol. *51*, p 1614.
(53) Yesiltas, M.; Glotch, T. D.; Jaret, S.; Verchovsky, A. B.; Greenwood, R. C. Carbonaceous matter in the Sariçiçek meteorite. *Meteorit. Planet. Sci.* **2019**, *54* (7), 1495−1511.
(54) Yesiltas, M.; Kaya, M.; Glotch, T. D.; Brunetto, R.; Maturilli, A.; Helbert, J.; Ozel, M. E. Biconical reflectance, micro-Raman, and nano-FTIR spectroscopy of the Didim (H3−5) meteorite: Chemical content and molecular variations. *Meteorit. Planet. Sci.* **2020**, *55* (11), 2404−2421.
(55) Brearley, A. J. The action of water. *Meteorites and the early solar system II* **2006**, *943*, 587−624.
(56) King, A. J.; Schofield, P. F.; Russell, S. S. Type 1 aqueous alteration in CM carbonaceous chondrites: Implications for the evolution of water-rich asteroids. *Meteorit. Planet. Sci.* **2017**, *52* (6), 1197−1215.
(57) Baker, L.; Franchi, I. A.; Wright, I. P.; Pillinger, C. T. The oxygen isotopic composition of water from Tagish Lake: Its relationship to low-temperature phases and to other carbonaceous chondrites. *Meteorit. Planet. Sci.* **2002**, *37* (7), 977−985.
(58) Guo, W.; Eiler, J. M. Temperatures of aqueous alteration and evidence for methane generation on the parent bodies of the CM chondrites. *Geochim. Cosmochim. Acta* **2007**, *71* (22), 5565−5575.
(59) Young, J. M., Henkes, G. A.; Glotch, T. D. Tracing the Aqueous Alteration of Carbonaceous Chondrites via Carbonate Clumped Isotope and Raman Carbon Thermometry. *51st Lunar and Planetary Science Conference*, The Woodlands, Texas, March 16−20, 2020; p 2455.
(60) Endress, M.; Zinner, E.; Bischoff, A. Early aqueous activity on primitive meteorite parent bodies. *Nature* **1996**, *379* (6567), 701−703.
(61) de Leuw, S.; Rubin, A. E.; Schmitt, A. K.; Wasson, J. T. 53Mn−53Cr systematics of carbonates in CM chondrites: Implications for the timing and duration of aqueous alteration. *Geochim. Cosmochim. Acta* **2009**, *73* (24), 7433−7442.
(62) Fujiya, W.; Sugiura, N.; Hotta, H.; Ichimura, K.; Sano, Y. Evidence for the late formation of hydrous asteroids from young meteoritic carbonates. *Nat. Commun.* **2012**, *3* (1), 1−6.
(63) Ikeda, Y.; Noguchi, T.; Kimura, M. Petrology and mineralogy of the Yamato-86720 carbonaceous chondrite. *Sixteenth Symposium on Antarctic Meteorites. Proceedings of the NIPR Symposium*, Tokyo, Japan, June 5−7, 1991; National Institute of Polar Research, 1992; Vol. *5*, p 136.
(64) Zolensky, M. E.; Lipschutz, M. E.; Hiroi, T. Mineralogy of artificially heated carbonaceous chondrites. *Lunar Planet. Sci.* **1994**, *25*, 1567.
(65) Zolensky, M. E., Mikouchi, T., Hagiya, K., Ohsumi, K., Komatsu, M., Chan, Q. H. S., Le, L., Kring, D., Cato, M., Fagan, A. L.; Gross, J. Unique view of C asteroid regolith from the Jbilet Winselwan CM chondrite. *47th Lunar and Planetary Science Conference* (CD-ROM), The Woodlands, Texas, March 21−25, 2016; Abstract 2148.
(66) Nakamura, T. Post-hydration thermal metamorphism of carbonaceous chondrites. *J. Mineral. Petrol. Sci.* **2005**, *100*, 260−272.
(67) Lee, M. R.; Lindgren, P.; King, A. J.; Greenwood, R. C.; Franchi, I. A.; Sparkes, R. Elephant Moraine 96029, a very mildly aqueously altered and heated CM carbonaceous chondrite: Implications for the drivers of parent body processing. *Geochim. Cosmochim. Acta* **2016**, *187*, 237−259.
(68) Kitajima, F.; Nakamura, T.; Takaoka, N.; Murae, T. Evaluating the thermal metamorphism of CM chondrites by using the pyrolytic behavior of carbonaceous macromolecular matter. *Geochim. Cosmochim. Acta* **2002**, *66* (1), 163−172.
(69) Gattacceca, J.; McCubbin, F. M.; Bouvier, A.; Grossman, J. N. The meteoritical bulletin, no. 108. *Meteorit. Planet. Sci.* **2020**, *55* (5), 1146−1150.
(70) Pizzarello, S.; Yarnes, C. T.; Cooper, G. The Aguas Zarcas (CM2) meteorite: New insights into early solar system organic chemistry. *Meteorit. Planet. Sci.* **2020**, *55* (7), 1525−1538.
(71) Kerraouch, I.; Bischoff, A.; Zolensky, M. E.; Pack, A.; Patzek, M.; Hanna, R. D.; Fries, M. D.; Harries, D.; Kebukawa, Y.; Le, L.; Ito, M.; Rahman, Z. The polymict carbonaceous breccia Aguas Zarcas: A potential analog to samples being returned by the OSIRIS-REx and Hayabusa2 missions. *Meteorit. Planet. Sci.* **2021**, *56* (2), 277−310.
(72) Kerraouch, I.; Bischoff, A.; Zolensky, M. E.; Pack, A.; Patzek, M.; Wölfer, E.; Burkhardt, C.; Fries, M. Characteristics of a New Carbonaceous Chondrite, Metal-Rich-Lithology Found in the Carbonaceous Chondrite Breccia Aguas Zarcas. *51st Lunar and Planetary Science Conference*, The Woodlands, Texas, March 16−20, 2020; Abstract 2011.
(73) Grady, M. M.; Abernethy, F. A. J.; Verchovsky, A. B.; King, A. J.; Schofield, P. F.; Russell, S. S. The Jbilet Winselwan carbonaceous chondrite 2. Light element geochemistry: Strengthening the link between CM and CO meteorites?. *77th Annual Meteoritical Society Meeting*, Casablanca, Morocco, September 8-13, 2014; Abstract 5377.
(74) King, A. J.; Russell, S. S.; Schofield, P. F.; Humphreys-Williams, E. R.; Strekopytov, S.; Abernethy, F. A. J.; Verchovsky, A. B.; Grady, M. M. The alteration history of the Jbilet Winselwan CM carbonaceous chondrite: An analog for C-type asteroid sample return. *Meteorit. Planet. Sci.* **2018**, *54* (3), 521−543.
(75) Friend, P.; Hezel, D. C.; Barrat, J. A.; Zipfel, J.; Palme, H.; Metzler, K. Composition, petrology, and chondrule-matrix complementarity of the recently discovered Jbilet Winselwan CM2 chondrite. *Meteoritics & Planetary Science* **2018**, *53* (12), 2470−2491.
(76) Nakamura, T.; Iwata, T.; Kitasato, K.; Abe, M.; Osawa, T.; Matsuoka, M.; Nakauchi, Y.; Arai, Y.; Komatsu, M.; Hiroi, T.; Imae, N.; Yamaguchi, A.; Kojima, H. Reflectance spectra measurement of hydrated and dehydrated carbonaceous chondrites using the Near Infrared Spectrometer on Hayabusa 2 spacecraft. *37th Symposium on Antarctic Meteorites*, 2014; Abstract 315.
(77) Huth, F.; Govyadinov, A.; Amarie, S.; Nuansing, W.; Keilmann, F.; Hillenbrand, R. Nano-FTIR absorption spectroscopy of molecular fingerprints at 20 nm spatial resolution. *Nano Lett.* **2012**, *12* (8), 3973−3978.
(78) Amarie, S.; Zaslansky, P.; Kajihara, Y.; Griesshaber, E.; Schmahl, W. W.; Keilmann, F. Nano-FTIR chemical mapping of minerals in biological materials. *Beilstein J. Nanotechnol.* **2012**, *3* (1), 312−323.
(79) Amenabar, I.; Poly, S.; Goikoetxea, M.; Nuansing, W.; Lasch, P.; Hillenbrand, R. Hyperspectral infrared nanoimaging of organic samples based on Fourier transform infrared nanospectroscopy. *Nat. Commun.* **2017**, *8* (1), 1−10.
(80) Yesiltas, M.; Glotch, T. D.; Sava, B. Nano-FTIR spectroscopic identification of prebiotic carbonyl compounds in Dominion Range 08006 carbonaceous chondrite. *Sci. Rep.* **2021**, *11* (1), 1−9.
(81) Yesiltas, M.; Kebukawa, Y.; Peale, R. E.; Mattson, E.; Hirschmugl, C. J.; Jenniskens, P. Infrared imaging spectroscopy with micron resolution of Sutter's Mill meteorite grains. *Meteoritics & Planetary Science* **2014**, *49* (11), 2027−2037.
(82) Yesiltas, M.; Young, J.; Glotch, T. D. Thermal metamorphic history of Antarctic CV3 and CO3 chondrites inferred from the first- and second-order Raman peaks of polyaromatic organic carbon. *American Mineralogist* **2021**, *106* (4), 506−517.
(83) Socrates, G. *Infrared and Raman characteristic group frequencies: tables and charts*; John Wiley & Sons, 2004.
(84) Kebukawa, Y.; Kobayashi, H.; Urayama, N.; Baden, N.; Kondo, M.; Zolensky, M. E.; Kobayashi, K. Nanoscale infrared imaging analysis of carbonaceous chondrites to understand organic-mineral interactions during aqueous alteration. *Proc. Natl. Acad. Sci. U. S. A.* **2019**, *116* (3), 753−758.
(85) Nuevo, M.; Sandford, S. A.; Flynn, G. J.; Wirick, S. Mid-infrared study of stones from the Sutter's Mill meteorite. *Meteoritics & Planetary Science* **2014**, *49* (11), 2017−2026.

(86) Yesiltas, M.; Kebukawa, Y. Associations of organic matter with minerals in Tagish Lake meteorite via high spatial resolution synchrotron-based FTIR microspectroscopy. *Meteorit. Planet. Sci.* **2016**, *51* (3), 584−595.
(87) Salisbury, J. W.; D'Aria, D. M.; Jarosewich, E. Mid Infrared (2.5−13.5 microns) reflectance spectra of powdered stony meteorites. *Icarus* **1991**, *92*, 280.
(88) Yesiltas, M.; Sedlmair, J.; Peale, R. E.; Hirschmugl, C. J. Synchrotron-based three-dimensional Fourier-transform infrared spectro-microtomography of Murchison meteorite grain. *Appl. Spectrosc.* **2017**, *71* (6), 1198−1208.
(89) Glotch, T. D.; Edwards, C. S.; Yesiltas, M.; Shirley, K. A.; McDougall, D. S.; Kling, A. M.; Bandfield, J. L.; Herd, C. D. MGS-TES spectra suggest a basaltic component in the regolith of Phobos. *Journal of Geophysical Research: Planets* **2018**, *123* (10), 2467−2484.
(90) Tuinstra, F.; Koenig, J. L. Raman spectrum of graphite. *J. Chem. Phys.* **1970**, *53* (3), 1126−1130.
(91) Ferrari, A. C.; Robertson, J. Interpretation of Raman spectra of disordered and amorphous carbon. *Phys. Rev. B: Condens. Matter Mater. Phys.* **2000**, *61* (20), 14095.
(92) Starkey, N. A.; Franchi, I. A.; Alexander, C. M. O'D. A Raman spectroscopic study of organic matter in interplanetary dust particles and meteorites using multiple wavelength laser excitation. *Meteorit. Planet Sci.* **2013**, *48* (10), 1800−1822.
(93) Cody, G.D.; Alexander, C. M. O'D.; Yabuta, H.; Kilcoyne, A. L. D.; Araki, T.; Ade, H.; Dera, P.; Fogel, M.; Militzer, B.; Mysen, B. O. Organic thermometry for chondritic parent bodies. *Earth Planet. Sci. Lett.* **2008**, *272* (1−2), 446−455.
(94) Schmidt, J. S.; Hinrichs, R. Evaluation of terrestrial carbonaceous matter aromatization by Raman spectroscopy and its application to C chondrites. *Meteorit. Planet. Sci.* **2020**, *55* (4), 800−817.
(95) Busemann, H.; Alexander, C. M. O'D.; Nittler, L. R. Characterization of insoluble organic matter in primitive meteorites by microRaman spectroscopy. *Meteorit. Planet Sci.* **2007**, *42* (7−8), 1387−1416.
(96) Alexander, C. M. O'D.; Fogel, M.; Yabuta, H.; Cody, G. D. The origin and evolution of chondrites recorded in the elemental and isotopic compositions of their macromolecular organic matter. *Geochim. Cosmochim. Acta* **2007**, *71* (17), 4380−4403.
(97) Alexander, C. M. O'D.; Bowden, R.; Fogel, M. L.; Howard, K. T.; Herd, C. D. K.; Nittler, L. R. The provenances of asteroids, and their contributions to the volatile inventories of the terrestrial planets. *Science* **2012**, *337* (6095), 721−723.
(98) Alexander, C. M. O'D.; Cody, G. D.; Kebukawa, Y.; Bowden, R.; Fogel, M. L.; Kilcoyne, A. L. D.; Nittler, L. R.; Herd, C. D. K. Elemental, isotopic, and structural changes in Tagish Lake insoluble organic matter produced by parent body processes. *Meteorit. Planet. Sci.* **2014**, *49* (4), 503−525.
(99) Le Guillou, C.; Bernard, S.; Brearley, A. J.; Remusat, L. Evolution of organic matter in Orgueil, Murchison and Renazzo during parent body aqueous alteration: In situ investigations. *Geochim. Cosmochim. Acta* **2014**, *131*, 368−392.
(100) Dionnet, Z.; Aleon-Toppani, A.; Baklouti, D.; Borondics, F.; Brisset, F.; Djouadi, Z.; Sandt, C.; Brunetto, R. Organic and mineralogic heterogeneity of the Paris meteorite followed by FTIR hyperspectral imaging. *Meteoritics & Planetary Science* **2018**, *53* (12), 2608−2623.
(101) Vinogradoff, V.; Le Guillou, C.; Bernard, S.; Binet, L.; Cartigny, P.; Brearley, A. J.; Remusat, L. Paris vs. *Geochim. Cosmochim. Acta* **2017**, *212*, 234−252.
(102) Anders, E.; Hayatsu, R.; Studier, M. H. Organic Compounds in Meteorites: They may have formed in the solar nebula, by catalytic reactions of carbon monoxide, hydrogen, and ammonia. *Science* **1973**, *182* (4114), 781−790.
(103) Robert, F.; Epstein, S. The concentration and isotopic composition of hydrogen, carbon and nitrogen in carbonaceous meteorites. *Geochim. Cosmochim. Acta* **1982**, *46*, 81−95.
(104) Kerridge, J. F.; Chang, S.; Shipp, R. Isotopic characterisation of kerogen-like material in the Murchison carbonaceous chondrite. *Geochim. Cosmochim. Acta* **1987**, *51*, 2527−2540.
(105) Alexander, C. M. O'D.; Russell, S. S.; Arden, J. W.; Ash, R. D.; Grady, M. M.; Pillinger, C. T. The origin of chondritic macromolecular organic matter: a carbon and nitrogen isotope study. *Meteorit. Planet. Sci.* **1998**, *33* (4), 603−622.
(106) Floss, C.; Stadermann, F. J. High abundance of circumstellar and interstellar C-anomalous phases in the primitive CR3 chondrites QUE 99177 and MET 00426. *Astrophys. J.* **2009**, *697*, 1242−1255.
(107) Remusat, L.; Robert, F.; Meibom, A.; Mostefaoui, S.; Delpoux, O.; Binet, L.; Gourier, D.; Derenne, S. Proto-planetary disk chemistry recorded by D-rich organic radicals in carbonaceous chondrites. *Astrophys. J.* **2009**, *698*, 2087−2092.
(108) Vollmer, C.; Kepaptsoglou, D.; Leitner, J.; Busemann, H.; Spring, N. H.; Ramasse, Q. M.; Hoppe, P.; Nittler, L. R. Fluid-induced organic synthesis in the solar nebula recorded in extraterrestrial dust from meteorites. *Proc. Natl. Acad. Sci. U. S. A.* **2014**, *111* (43), 15338−15343.
(109) Kuga, M.; Marty, B.; Marrocchi, Y.; Tissandier, L. Synthesis of refractory organic matter in the ionized gas phase of the solar nebula. *Proc. Natl. Acad. Sci. U. S. A.* **2015**, *112* (23), 7129−7134.
(110) Yang, J.; Epstein, S. Interstellar organic matter in meteorites. *Geochim. Cosmochim. Acta* **1983**, *47* (12), 2199−2216.
(111) Theulé, P.; Duvernay, F.; Danger, G.; Borget, F.; Bossa, J. B.; Vinogradoff, V.; Mispelaer, F.; Chiavassa, T. Thermal reactions in interstellar ice: A step towards molecular complexity in the interstellar medium. *Adv. Space Res.* **2013**, *52* (8), 1567−1579.
(112) McBride, E. J.; Millar, T. J.; Kohanoff, J. J. Organic synthesis in the interstellar medium by low-energy carbon irradiation. *J. Phys. Chem. A* **2013**, *117* (39), 9666−9672.
(113) Spezia, R.; Jeanvoine, Y.; Hase, W. L.; Song, K.; Largo, A. Synthesis of formamide and related organic species in the interstellar medium via chemical dynamics simulations. *Astrophysical Journal* **2016**, *826* (2), 107.
(114) Abplanalp, M. J.; Kaiser, R. I. On the formation of complex organic molecules in the interstellar medium: untangling the chemical complexity of carbon monoxide−hydrocarbon containing ice analogues exposed to ionizing radiation via a combined infrared and reflectron time-of-flight analysis. *Phys. Chem. Chem. Phys.* **2019**, *21* (31), 16949−16980.
(115) Miller, S. L.; Urey, H. C.; Oro, J. Origin of organic compounds on the primitive earth and in meteorites. *J. Mol. Evol.* **1976**, *9* (1), 59−72.
(116) Schulte, M.; Shock, E. Coupled organic synthesis and mineral alteration on meteorite parent bodies. *Meteorit. Planet. Sci.* **2004**, *39* (9), 1577−1590.
(117) Cooper, G.; Reed, C.; Nguyen, D.; Carter, M.; Wang, Y. Detection and formation scenario of citric acid, pyruvic acid, and other possible metabolism precursors in carbonaceous meteorites. *Proc. Natl. Acad. Sci. U. S. A.* **2011**, *108* (34), 14015−14020.
(118) Remusat, L.; Palhol, F.; Robert, F.; Derenne, S.; France-Lanord, C. Enrichment of deuterium in insoluble organic matter from primitive meteorites: a solar system origin? *Earth Planet. Sci. Lett.* **2006**, *243*, 15−25.
(119) Gourier, D.; Robert, F.; Delpoux, O.; Binet, L.; Vezin, H.; Moissette, A.; Derenne, S. Extreme deuterium enrichment of organic radicals in the Orgueil meteorite: revisiting the interstellar interpretation? *Geochim. Cosmochim. Acta* **2008**, *72*, 1914−1923.
(120) Cody, G. D.; Heying, E.; Alexander, C. M. O'D.; Nittler, L. R.; Kilcoyne, A. L. D.; Sandford, S. A.; Stroud, R. M. Establishing a molecular relationship between chondritic and cometary organic solids. *Proc. Natl. Acad. Sci. U. S. A.* **2011**, *108* (48), 19171−19176.
(121) Alexander, C. M. O'D.; Cody, G. D.; De Gregorio, B. T.; Nittler, L. R.; Stroud, R. M. The nature, origin and modification of insoluble organic matter in chondrites, the major source of Earth's C and N. *Chem. Erde* **2017**, *77* (2), 227−256.
(122) Metzler, K.; Bischoff, A. Evidence for Aqueous Alteration Prior to Parent Body Formation; Petrographic Observations in CM-Chondrites. *Lunar and Planetary Science Conference*, 1991; Vol. *22*, p 893.

(123) Krot, A. N.; Scott, E. R.; Zolensky, M. E. Mineralogical and chemical modification of components in CV3 chondrites: Nebular or asteroidal processing? *Meteoritics* **1995**, *30* (6), 748−775.
(124) Krot, A. N.; Petaev, M. I.; Scott, E. R.; Choi, B. G.; Zolensky, M. E.; Keil, K. Progressive alteration in CV3 chondrites: More evidence for asteroidal alteration. *Meteorit. Planet. Sci.* **1998**, *33* (5), 1065−1085.
(125) Hanowski, N. P.; Brearley, A. J. Iron-rich aureoles in the CM carbonaceous chondrites Murray, Murchison, and Allan Hills 81002: Evidence for in situ aqueous alteration. *Meteorit. Planet. Sci.* **2000**, *35* (6), 1291−1308.
(126) Browning, L.; McSween Jr, H. Y.; Zolensky, M. E. On the origin of rim textures surrounding anhydrous silicate grains in CM carbonaceous chondrites. *Meteorit. Planet. Sci.* **2000**, *35* (5), 1015−1023.
(127) Dartois, E.; Muñoz-Caro, G. M. Carbonaceous dust grains in luminous infrared galaxies-Spitzer/IRS reveals aC: H as an abundant and ubiquitous ISM component. *Astron. Astrophys.* **2007**, *476* (3), 1235−1242.
(128) Pino, T.; Cao, A. T.; Carpentier, Y.; Dartois, E.; d'Hendecourt, L.; Bréchignac, P. Laboratory analogues of hydrocarbonated interstellar nanograins. *Proc. Int. Astron. Union* **2008**, *4*, 393−394.
(129) Gadallah, K. A. K.; Mutschke, H.; Jäger, C. UV irradiated hydrogenated amorphous carbon (HAC) materials as a carrier candidate of the interstellar UV bump at 217.5 nm. *Astron. Astrophys.* **2011**, *528*, A56.


https://doi.org/10.1021/acsearthspacechem.1c00290
*ACS Earth Space Chem.* 2021, 5, 3281−3296